Rijksuniversiteit Groningen

BSc Astronomy

Dust and Star Formation in Early-type Dwarf Elliptical Galaxies in the Fornax- and Virgo Cluster

Author:
A. H. Corporaal

Supervisor:
R. F. Peletier
L. Wang

July 10, 2017

Abstract

Physical properties of dust in early-type dwarf elliptical galaxies (dEs) in the Fornax- and Virgo cluster have been determined by using Spectral Energy Distribution (SED) modelling. 6 objects in the Fornax cluster and 19 objects in the Virgo cluster have been detected using the Wide-Field Infrared Survey Explorer (*WISE*) and the *Herschel* Space Observatory. For these galaxies dust temperature, integrated infrared luminosity, star formation rate and an rough estimate for the stellar mass are determined. In addition, the dust masses are determined for 4 galaxies in the Fornax cluster and for 4 galaxies in the Virgo cluster. The physical properties for the Fornax cluster and the Virgo cluster are comparable within the uncertainties. It was found the dwarf ellipticals in the sample have a significant dust content. Upper limits on the flux densities, however, are not taken into account in this research.

Contents

1 Introduction

1.1 Dwarf elliptical galaxies

Dwarf galaxies are the dominant type of galaxy in the universe. Dwarf galaxies are relatively small galaxies with a relatively low mass and are usually companions of other galaxies (Sparke and Gallagher, 2007). They are rarely found in the field, but are common in clusters of galaxies. Dwarf galaxies can be distinguished into different types: dwarf elliptical galaxies (dEs), dwarf spheroidal galaxies (dSph), dwarf irregular galaxies (dIrr), dwarf spirals galaxies (dS), blue compact dwarf galaxies (BCDs) and ultra-compact dwarf galaxies (UCD). In addition, Sandage & Binggeli (1984) proposed the class of dwarf lenticular galaxies, dS0's. dS0's are originally considered to be like giant lenticular galaxies having a bulge and disc component (Sandage & Binggeli, 1984). Both dS0's and dEs are characterised by the assumption that they lost or used up most of their dust and gas to form stars. Both are considered to be early-type galaxies and following the common definition, both dwarf elliptical galaxies and dS0's are included in the abbreviation dE. This thesis concentrates on the dEs.

Early-type dwarf elliptical galaxies are relatively small elliptical galaxies with a relatively low surface brightness. dEs are characterised by a smooth intensity distribution (Sandage & Binggeli, 1984). The distinction between a giant elliptical galaxy and a dwarf elliptical galaxy originates from total blue magnitude (Sandage & Binggeli, 1984). An elliptical galaxy that has an absolute blue magnitude $M_B > -18$ is catagorised as an early-type dwarf elliptical galaxy while a giant elliptical galaxy has $M_B < -18$ (Sandage & Binggeli, 1984).

1.1.1 Scaling relations

Scaling relations can be used to compare different types of galaxies with each other and to study the kinematics and the stellar population of the galaxy (Boselli et al., 2008). Some scaling relations between giant elliptical galaxies and dwarf elliptical galaxies are considered.

The upper left plot in Fig. 1 shows the surface brightness versus the absolute blue magnitude for early-type galaxies. It shows that the surface brightness of giant elliptical galaxies and S0's increases as the total luminosity decreases whereas the surface brightness of dwarf elliptical galaxies decreases as the total luminosity decreases. The surface brightness profile of a giant elliptical galaxy described by a de Vaucouleurs' law while dEs have an exponentially declining surface brightness profile. The upper right plot in Fig. 1 shows the Kormendy relation, which indicates how the effective radius scales with surface brightness.

The lower left plot in Fig. 1 shows the relation between the absolute blue magnitude of a galaxy and the effective radius. For giant elliptical galaxies the effective radius increases with increasing luminosity, while for dwarf elliptical galaxies the effective radius remains constant over the absolute magnitude range ($M_B > -18$ for dEs).

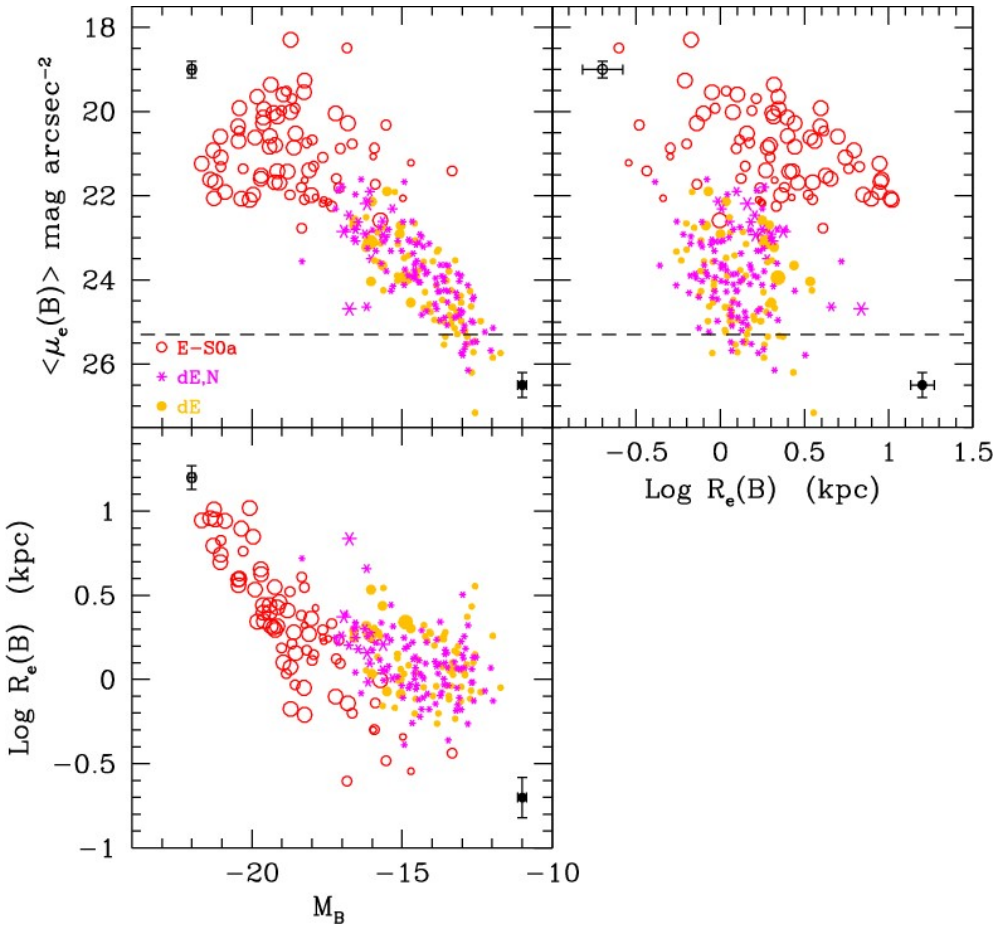

Figure 1: Plots of the scaling relations for early-type galaxies. Upper left: the effective brightness versus the B band absolute magnitude. Upper right: the Kormendy relation. Lower left: the radius versus the absolute B band magnitude. Red open circles represent giant ellipticals and lenticular galaxies, magenta asterisks represent nucleated dEs and orange filled dots represent dEs. (Boselli et al. 2008).

Plots of these scaling relations for late-type galaxies are shown in Fig. 2. The upper left plot in Fig. 2 shows that the surface brightness for spiral galaxies decreases as the total luminosity decreases. This is similar to the relation between the surface brightness and the luminosity for dwarf elliptical galaxies. The upper right plot shows the Kormendy relation for spiral and irregular galaxies. This relation is almost the same for late-type irregular galaxies and dEs. The lower left plot in Fig. 2 shows the relation between the luminosity and the effective radius and for this relation, a comparison between early-type galaxies and late-type galaxies is harder to make, since there is more scatter for the late-type irregular galaxies than for the dEs in Fig. 1. The irregular galaxies and the Sa-Sc galaxies have a relative large overlapping region, but the relation seems to be similar to giant elliptical galaxies: the effective radius increases with increasing luminosity. From the comparison between the scaling relations for early-type galaxies as shown in Fig. 1 and the scaling relations for late-type galaxies as shown in Fig. 2, it can be concluded that these relations are to a large extend similar for early-type elliptical dwarf galaxies and late-type galaxies.

However these late-type galaxies are star forming galaxies, whereas dEs are originally considered to be gas- and dust poor galaxies without ongoing or recent star formation. In section 1.2 a discussion on this is elucidated.

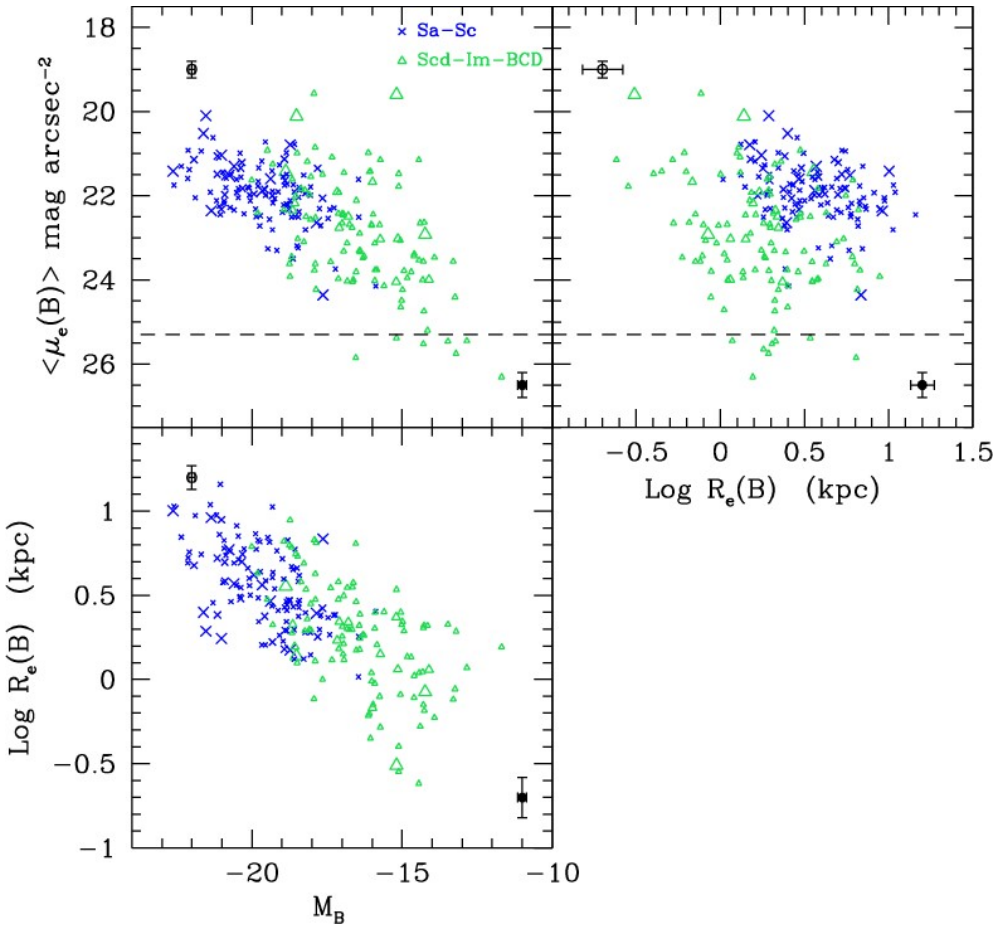

Figure 2: Plots of the scaling relations for late-type galaxies. Upper left: the effective brightness versus the B band absolute magnitude. Upper right: the Kormendy relation. Lower left: the radius versus the absolute B band magnitude. Blue crosses represent Sa-Sc galaxies, green triangles represent Scd-Im-BCD galaxies. Figure taken from Boselli et al. (2008).

1.1.2 Formation and evolution of dwarf elliptical galaxies

The formation and evolution of dEs is much debated. Dressler (1980) presented the morphology-density relation, which is an observationally determined relation between the morphology of a galaxy and the environment in which the galaxy is located. The environment here means how many galaxies are located near the galaxy in question and is represented by a density, mostly given in number of galaxies per cubic megaparsec. The morphology-density relation indicates that early-type galaxies (ellipticals and S0's) are located in the denser cluster core while the less dense outskirts of galaxy clusters are dominated by spiral galaxies and irregular galaxies. The morphology-density relation is shown in Fig. 3 (Dresser, 1980). The fraction of the different morphologies as a function of the logarithm of the projected density is plotted.

The difference in environmental density in the cluster between early-type galaxies and late-type galaxies can be explained by environmental processes. Spirals that are falling in into the denser parts of the cluster could lose part of their gas and turn into S0's. As a result of the morphology-density relation, it is believed that the evolution of a galaxy is affected by the environment in which a galaxy is located.

Such evolutionary processes could also be true at smaller scales. dIrr are believed to be gas rich, while dEs are believed to be gas-poor. dIrr that fall into the denser parts of the cluster can be morphologically transformed to dEs (Lisker et al., 2007) and late-type spiral galaxies can also fall into the denser parts of the cluster and be perturbed in such a way that features change to

dEs (Boselli et al., 2008). Skillman et al. (2003) noticed that dIrr and dEs are very similar in star formation up to the point where dEs lose their gas. Drinkwater et al. (2001b) pointed out that their sample of galaxies shows indeed a cluster core that is devoid of star forming dwarfs.

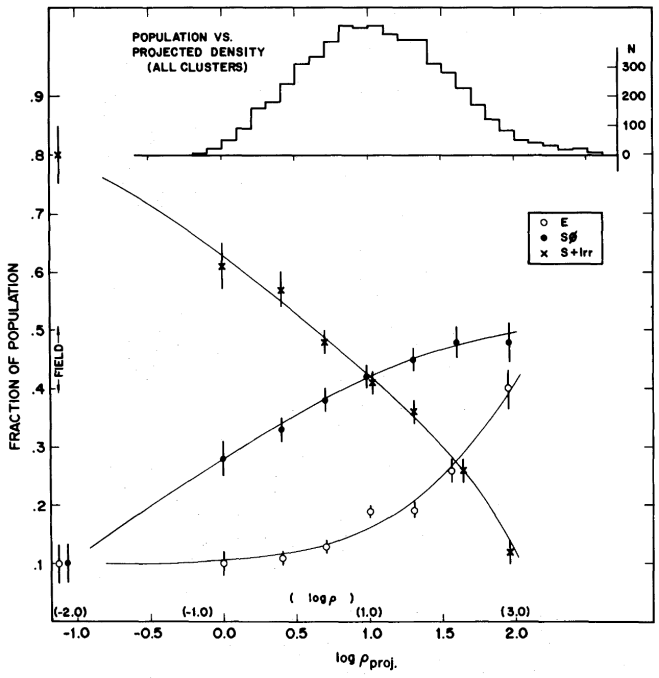

Figure 3: Fraction of elliptical galaxies (E), S0 galaxies, spiral galaxies and irregular galaxies as a function of the logarithm of the projected density in Mpc^{-2} estimate for the logarithm of the true density is given above the horizontal axis. The histogram on top shows the number of galaxies in the bins of projected density (Dressler, 1980).

Environmental effects such as ram pressure stripping (Gunn & Gott, 1972), galaxy harassment (Moore et al., 1996) and tidal stirring (Mayer et al., 2001) are believed to tear away the gas and dust from the galaxy, leading to the smooth appearance of the dE (Lisker et al., 2006). Ram pressure stripping is the process in which a galaxy that is moving through the intracluster medium experiences a pressure that is higher than the pressure holding the gas bound to the galaxy and therefore loses the gas (Gunn & Gott, 1974). This is the case if a spiral galaxy or an irregular galaxy moves through the denser parts of the cluster. An impression of ram pressure stripping is shown in Fig. 4. NGC 4569 is located close to the center of the Virgo cluster and it is shown how the ionised tails of the lost gas are oriented.

In the case of galaxy harassment, a galaxy is affected by a fly-by of a bigger galaxy and this type of galaxy interaction affects especially the outer parts of the galaxy. This should not be confused with mergers of galaxies, as was shown in simulations by Moore et al. (1996). Such fly-bys can disturb or even transform the morphology of a galaxy. This process can also trigger star formation. Tidal forces from larger galaxies or from the cluster core can also trigger morphological transformations, Mayer er al. discussed this effect on the basis of the Local Group and stated that this environmental process could also have an effect on poor clusters such as Fornax and Virgo (Drinkwater et al., 2001b). These environmental effects are believed to be one of the mechanism for the formation and evolution of dwarf elliptical galaxies.

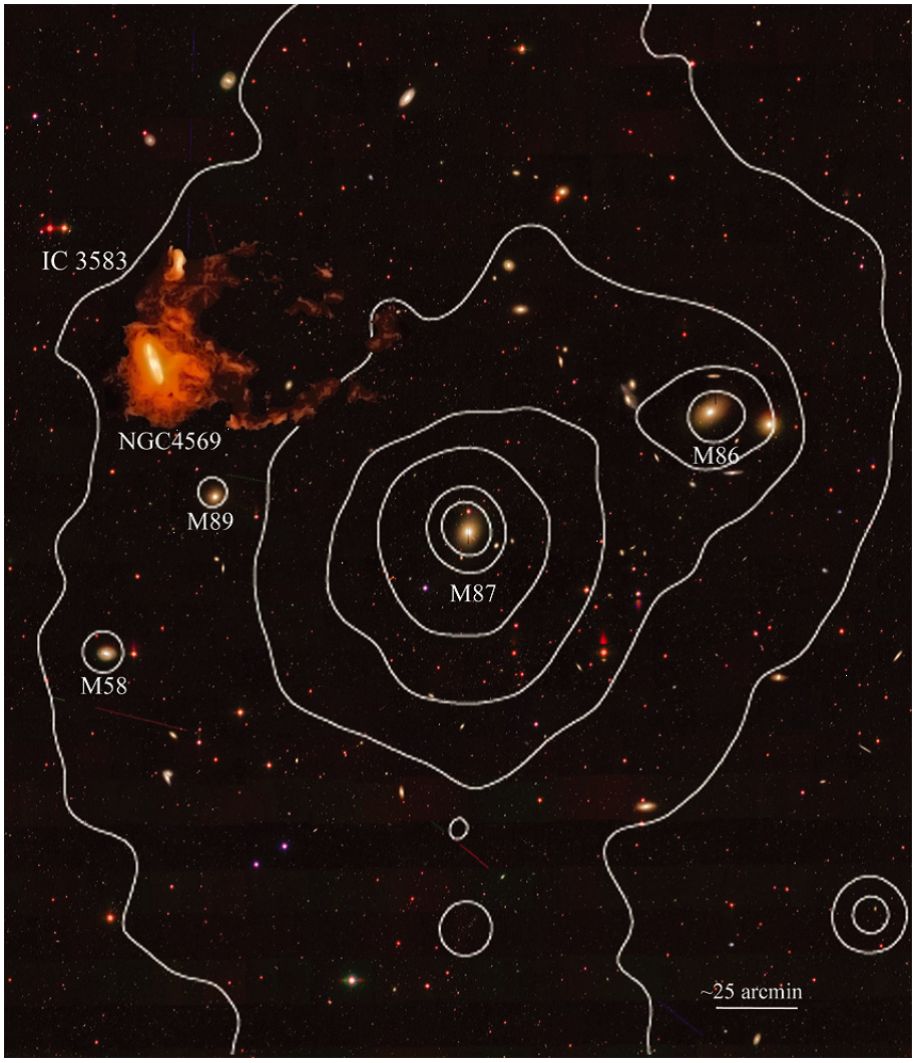

Figure 4: Illustration of ram pressure stripping of NGC 4569. NGC 4569 is located at a distance of 1.7 degrees from the central elliptical galaxy of the Virgo cluster, M87. The emphasise is on the orientation of the tail of the ionised gas with respect to the location of the galaxy in the cluster. (Boselli et al., 2016)

1.2 Dust, gas and star formation

Are stars currently being formed in dwarf elliptical galaxies? One of the indicators is the discovery of dwarf ellipticals in the Virgo cluster having blue centers (Lisker et al. 2006b). These blue centers indicate that stars are currently forming or must have formed in the recent past as the blue regions originates from young and hot stars.

Dust and gas in a galaxy are associated with star formation. Interstellar dust determines what galaxies look like and how the interstellar medium (ISM) behaves (Draine, 2003). Dust is closely connected to the evolution of a galaxy and originates from supernova explosions of massive stars and active galactic nuclei (Draine, 2003). Dust is a catalyst in the process of transforming atomic hydrogen into molecular hydrogen (Draine, 2003). Molecules such as molecular hydrogen are needed to form the molecular clouds where under high densities and low temperatures stars can form. Cold gas and dust are fuel to star formation in galaxies. Because of the dust that is present in the region around the hot O and B stars, this ultraviolet (UV) light radiated by hot O and B stars is absorbed by dust and re-radiated in the infrared (IR) and in the sub-millimeter (submm) parts of the spectrum. In these parts of the spectrum the thermal emission of grains is dominant and this dominates the spectral energy distribution (SED) between 8 and 1000 μm. To

trace ISM in galaxies, dust emission is frequently used.

UV radiation is energetic enough to ionise the atoms, molecules and ions that are present in the surrounding ISM. The free electrons originating from these atoms, molecules and ions will recombine with the ions and energy is emitted at a specific wavelength of radiation. These lines in an emission spectrum are called emission lines of a certain atom, ion or molecule. If an emission spectrum of a galaxy can be taken, the chemical composition of the galaxy can be determined. The emission lines produced by the hot and massive O and B stars are tracers of star formation in these galaxies which indicates that star formation can be an ongoing process.

Although it is thought that the environmental effects should remove all the gas from dwarf elliptical galaxies, the discovery of dEs with blue centers and the observation of dust in dwarf elliptical galaxies changed the view of dEs having no recent or ongoing star formation (Lisker et al., 2006b). That means that it likely that there is some kind of ISM in dEs. In this research project we look at the number of dwarf ellipticals in the Fornax cluster and the Virgo cluster for which we can find ISM traces by using the Wide-Field Infrared Survey Explorer (*WISE*) and the *Herschel* Space Observatory. These space telescopes have measured continuum emission from interstellar dust at various wavelengths.

Although dEs are the most common galaxy type in the nearby galaxies clusters, the basic properties of the dust are not quantified. This is due to the fact that the detection of gas in dEs is difficult because dEs are small and have a low surface brightness. This makes HI and molecular observations difficult. In this thesis some physical parameters of the dust in dEs will be derived using *WISE* and *Herschel* observations.

The data and sample selection is described in section 2, followed by the description of the SED modelling in section 3. The results and an analysis of the SED fitting is the subject of section 4. A discussion on the relation between the detection probability and the location where a galaxy if found in the cluster is presented in section 5. Section 5 also includes comparisons with literature. Section 6 presents the conclusions and states some recommendations for further research.

2 Data and sample selection

2.1 Data collection

The data was collected using the NASA/IPAC Infrared Science Archive (IRSA) which put together the science products that were collected by the National Aeronautics and Space Administration (NASA) IR and submm missions (IRSA, 2017). IRSA provides tools to search in the *Herschel* archive as well.

2.1.1 *WISE*

The 40 cm *WISE* telescope was launched by NASA in December 2009 and operates in the infrared. *WISE*is an all-sky survey centered at 3.4, 4.6, 12 and 22 microns. These bands are referred to as W1, W2, W3 and W4 respectively. The bands have an angular resolution of 6.1", 6.4", 6.5" and 12.0" respectively and typical 5σ sensitivity levels of 0.08, 0.11, 1 and 6 mJy (Wright et al., 2010). The All-Sky Data release archived in IRSA was used to collect the *WISE* data. This data was taken in the cryogenic phase of the *WISE* mission (Wright et al., 2010) and the fluxes given in this catalogue are in units of magnitudes.

In Fig. 5 a Spectral Energy Distribution (SED) for the wavelength range 1 μm to 1000 μm is shown. It is shown that for the wavelengths corresponding to the W1 and W2 bands young stars are important contributions and therefore W1 and W2 are stellar colours. As a result the W1 and

W2 bands are less interesting for the research whether there is ongoing or recent star formation in dEs. The W3 band is sensitive to polycyclic aromatic hydrocarbon (PAH) emission from photon-dominated regions which comes from recent star formation. Furthermore Fig. 4 shows that the W4 band is sensitive to warm dust emission which is excited by star formation.

2.1.2 *Herschel*

The 3.5m *Herschel* Space Observatory was launched by the European Space Agency (ESA) and observed in far-infrared (FIR) and submillimeter wavelengths. *Herschel* carried three instruments: the Heterodyne Instrument for the Far Infrared (HIFI), the Photoconductor Array Camera and Spectrometer (PACS) and the Spectral and Photometric Imaging Receiver (SPIRE). HIFI is a high resolution spectrograph, while PACS and SPIRE both are cameras. PACS observed in three bands centered at 70, 100 and 160 microns with a spatial resolution of 5.5", 6.7" and 11" respectively (Marton et al., 2017). SPIRE observed in band centered at 250, 350 and 500 microns with a spatial resolution of 17.9", 24.2" and 35.4" respectively (Schultz et al., 2007). The PACS and SPIRE point source catalogues archived in IRSA are used to collect the data. The flux densities given in these catalogues are in units of mJy.

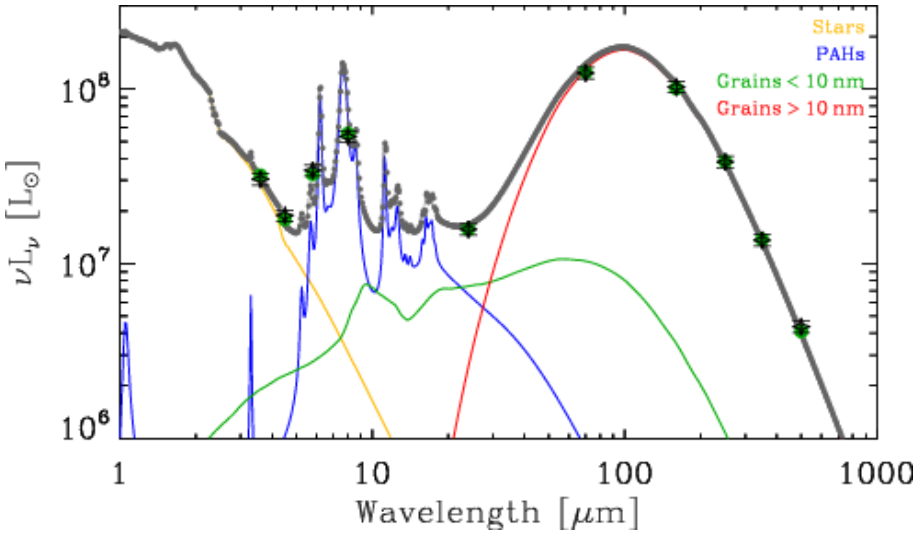

Figure 5: Spectral Energy Distribution for the observed wavelengths between1 μm and 1000 μm. The yellow line shows where the young stars contribute to the SED. The blue line indicates where PAHs contribute and the green and red lines indicate where grains with sizes <10 nm and >10 nm respectively dominate. (Meixner et al., 2010)

2.2 Sample selection

2.2.1 Fornax

Fornax is a cluster of galaxies that is 20 ± 0.2 Mpc away from us (Blakeslee et al., 2009). It is located away from the Galactic plane with Galactic latitude of -54.6 degrees in an area where there is no foreground ISM (Fuller et al. 2014). Fornax has a virial radius of 0.7 Mpc (2 °) (Drinkwater et al., 2001).

The Fornax Cluster Catalog (FCC) of Ferguson (1989) was used. The FCC is a catalogue of 2678 galaxies of which 2338 are likely background galaxies and 340 are likely Fornax cluster members (Ferguson, 1989). The FCC was created by visually inspecting both the photographic plates taken with the Du Pont 2.5m reflector at the Las Campanas Observatory and digital photometry of a blue survey plate (Ferguson, 1989). These galaxies are located in an area of approximately 40

square degrees centered on a Right Ascension (RA) around ≈ 3h35m and a declination (DEC) around ≈ −35.7°.

The FCC is considered to be complete to an apparent blue magnitude $m_B \approx 18$ (corresponding to $M_B \approx -13.5$) and considers members up to $m_B \approx 20$ (corresponding to $M_B \approx -11.5$). M_B is determined assuming that the distance modulus for the Fornax cluster $(m - M)_{Fornax}$=31.5.

NGC 1399 is the central giant elliptical galaxy of the Fornax cluster and is located α= 03h38m29.0s and δ=-35d27m02s in Equatorial J2000 coordinates. All galaxies catalogued as (likely) Fornax cluster members within 4 degrees from NGC 1399 were used as a full sample. This covers the virial radius of the Fornax cluster.

2.2.2 Virgo

The Fornax cluster will be compared to the Virgo cluster, which is located at a distance of 16.5 ± 0.1 Mpc (Mei et al., 2007). The Virgo cluster is the closest galaxy cluster to the Milky Way and has a viral radius of approximately 1.6 Mpc (5.6 °) (Mamon et al., 2004). The Virgo Cluster Catalog (VCC) was taken from Binggeli et al. (1985) and is equivalent to the FCC. The VCC was created by inspecting 67 blue plates taken between 1979 and 1982 with the du Pont 2.5 m reflector of the Las Campanas Observatory. The VCC contains 2096 galaxies within an area of approximately 140 square degrees (Binggeli et al., 1985). Of these 2096 galaxies, 1277 are catalogued as cluster members, 574 galaxies are possible members and 245 are background galaxies. The catalogue is centered at $\alpha \approx$ 12h25m and $\delta \approx 13°$.

The VCC is considered to be complete up to $m_B \approx 18$ (corresponding to $M_B \approx -13.1$) and considered members up to $m_B \approx 20$ (corresponding to $M_B \approx -11.1$), where M_B is determined assuming the distance modulus for the Virgo cluster $(m - M)_{Virgo}$=31.1. M87 is a giant elliptical galaxy in the center of the Virgo cluster with α= 12h30m49.4s and δ=+12d23m28s. All galaxies within 6 degrees from M87 were used as a full sample. This covers the viral radius of the Virgo cluster.

Both the FCC and the VCC based the membership of the galaxies to a large extend on galaxy morphology. This has essentially no effect on the membership of dwarf galaxies, since they are characterised by a low surface brightness. However for spirals and ellipticals the designation of membership could be uncertain and their membership also relies on velocities of the galaxies.

2.2.3 Selection of dwarf ellipticals

The FCC and VCC were used separately for cross matching between the galaxies and the *WISE* and *Herschel* data. All galaxies that are (likely) members of the Fornax- or Virgo cluster within a cone radius of 4 degrees from NGC 1399 and 6 degrees from M87 were used. This results in a full sample that consist of 328 FCC galaxies and 1542 VCC galaxies. Galaxies that were classified in the FCC and VCC as (possible) dE and dS0 were selected. This includes peculiar dwarf elliptical galaxies (dE pec), dEs with an uncertain classification (i.e. dE? or dE:) and nucleated dEs (dE, N). The morphological designation was checked by using the distance modulus and the apparent blue magnitude, m_B, and the definition of a dE (i.e. $M_B > -18$). Using the distance modulus of Fornax, this means that $M_B > -18$ if $m_B > 13.5$. From the distance modulus of the Virgo cluster, $M_B > -18$ corresponds to $m_B > 13.1$. This results in a sample containing 251 dEs in the Fornax cluster, corresponding to 77% ± 3% of the galaxies catalogued as (likely) cluster members in the covered area of the FCC. The sample for the Virgo cluster consist of 1049 dEs, corresponding to 68% ± 1% of the galaxies catalogued as (possible) members of the Virgo cluster in the covered area of the VCC.

A cone search radius of 15 arcsec was used to search in the IRSA database. This radius was determined from optical images of the galaxies such that it is unreasonable to get other sources in the covered radius. However, since the FCC and VCC rely on optical data, there is a risk of missing sources that are detected in the FIR but not in the optical. All detections in the *WISE* and *Herschel* bands within a radius of 15" from the rights ascensions and declinations given for the dEs are found in the IRSA databases.

From these samples, all galaxies that have a W3 error or a W4 error are selected, meaning that these galaxies have a detection in those bands. Similarly, all galaxies that have an error in one or more *Herschel* bands are selected. 60 FCC dEs that have either a W3, W4 or a detection in one of the *Herschel* bands are selected. This corresponds to 24% ± 3% of the dEs in the sample of Fornax galaxies. For the dwarf elliptical galaxies in the Virgo cluster 222 galaxies are selected, corresponding to 21% ± 2% of the dEs in the sample of Virgo galaxies.

2.2.4 Selection based on *WISE* and *Herschel*

In order to estimate the temperature, a composite function of a greybody and a power law (see section 3) was fitted for every galaxy that was detected in at least 2 bands: at least in one *WISE* band and at least in one *Herschel* band, not counting the W1 and W2 detections. This selection condition is needed since the number of free parameters in a least-squares fitting procedure cannot exceed the number of data points. This requirement means that the not all galaxies in the full sample are used. Appendix 1 list the VCC and FCC numbers that are not used because of the requirement for having at least one detection in the W3 or W4 band and at least one detection in the *Herschel* bands. In addition FCC 17, FCC 129, VCC 88, VCC 964, VCC 1272 and VCC 1445 were excluded because the radial velocity data that was available was over 3000 km/s, meaning that these galaxies are probably not cluster members.

This results in a sample of 6 galaxies located in the Fornax cluster and 19 galaxies located in the Virgo cluster that can be used for the SED fitting to determine the dust temperature. For the Fornax cluster this corresponds to 3% ± 1% of the dEs catalogued in the FCC as certain or likely cluster members and 10% ± 4% of the dEs having at least one detection in the W3, W4 or one of the *Herschel* bands. For the Virgo cluster this corresponds to 2% ± 1% of the dEs catalogued as certain or possible cluster members and to 9% ± 1% of the dEs having at least one detection in the W3 or W4 or at least one detection in the *Herschel* bands. This significant lower number of detections is because the selection of dwarf ellipticals contains a lot of galaxies that are only detected in W3. The dwarf elliptical galaxies have a low surface brightness and are therefore not often detected in the W4 and the *Herschel* bands.

The spectral features of the galaxies are shifted because we observe from a distance. The wavelengths at which the galaxies are observed are not the wavelengths at which these galaxies emitted their spectral features. Therefore the wavelength should be corrected for using the redshifts, z, of the individual galaxies. The redshifts for the galaxies are taken from the NASA/IPAC Extragalactic Database (NED).

Some dEs in the sample do not have available redshift data. For these galaxies, it is assumed that the redshift is equal to the redshift of the cluster. Drinkwater et al. (2000) determined that the average radial velocity from 26 cluster members in the Fornax cluster with reliable redshift data is 1560 ± 80 km/s. This corresponds to $< z >= 0.0052$. The average radial velocity for the Virgo cluster was determined to be 863 km/s by Arp (1988). This corresponds to $< z >= 0.0029$

In Table 1 the sample of the dEs located in the Fornax cluster is presented. The right ascension and declination of each galaxy are given in the J2000 coordinate system and are taken from NED.

Moreover, the type as taken form the FCC and the redshift of each galaxy are shown. The distance to the central galaxy, r, is given in units of degrees.

The sample of dEs located in the Virgo cluster for which the dust temperature can be determined is shown in Table 2. The right ascension and declination of the galaxies are given in J2000 coordinates and the type of the galaxies as given in the VCC are used. The redshift and the distance from the central galaxy M87 are also given.

Object	RA [1] h:m:s (J2000)	DEC [1] d:m:s (J2000)	type [2]	z [3]	r (deg)
FCC 32	03:24:52.4	-35:26:08	dE pec/BCD	0.004396	3.4
FCC 84	03:30:36.6	-35:02:29	dE0,N	0.0052*	2.0
FCC 207	03:38:19.3	-35:07:45	dE2,N	0.004737	0.3
FCC 215	03:38:37.6	-35:45:27	dE,N?	0.006551	0.3
FCC 261	03:41:21.5	-33:46:09	dE3 pec / ImIv	0.004977	1.8
FCC 282	03:42:45.3	-33.55:14	ImIv/dEpec	0.004086	1.9

Table 1: The sample for the Fornax cluster dwarf elliptical galaxies. The N in the column 'type' is an abbreviation for nucleated. This means that the dwarf elliptical is nucleated
[1] Data taken from NED.
[2] Data taken from Binggeli et al., 1985.
[3] Data taken from NED. A '*' in the redshift column means that the redshift is taken as the average redshift of the cluster

Object	RA [1] h:m:s (J2000)	DEC [1] d:m:s (J2000)	type [2]	z [3]	r (deg)
VCC 112	12:14:29.6	14:04:36	dE7?	0.0029*	4.4
VCC 170	12:15:56.3	14:25:59	dS0 pec	0.004707	4.2
VCC 184	12:16:18.7	09:44:49	dE0?,N	0.0047313	4.5
VCC 209	12:16:52.3	14:30:52	dS0	0.00429	4.1
VCC 218	12:17:05.5	12:17:23	dS08,N	0.001778	3.4
VCC 281	12:18:15.3	13:44:57	dS0/BCD	0.000809	3.4
VCC 560	12:22:31.6	11:48:09	dE2:,N	0.004646	2.2
VCC 645	12:23:31.6	11:16:14	dE0,N	0.0029*	2.1
VCC 774	12:25:10.0	10:27:24	dE0	0.0029*	1.4
VCC 781	12:25:15.2	12:42:53	dS035N:	-0.000627	1.4
VCC 898	12:26:23.6	13:22:25	dE0?	0.0029*	1.5
VCC 903	12:26:28.0	12:55:14	dE02,N	0.0029*	1.2
VCC 1420	12:32:12.2	12:03:42	dE4,N	0.003336	0.5
VCC 1447	12:32:38.6	10:45:34	dE4?,N	0.0029*	1.7
VCC 1453	12:32:44.2	14:11:46	dE2,N	0.006501	1.9
VCC 1463	12:32:54.0	12:48:28	dE3	0.0029*	0.7
VCC 1502	12:33:25.1	13:25:02	dE3	0.0029*	1.2
VCC 1577	12:34:38.4	15:36:10	dE4	0.001204	3.4
VCC 1749	12:38:12.1	10:42:07	dE0,N	0.0029*	2.5

Table 2: The sample for the Virgo cluster dwarf elliptical galaxies. The N in the column 'type' means nucleated, meaning that the dwarf elliptical is nucleated.
[1] Data taken from NED.
[2] Data taken from Binggeli et al., 1985.
[3] Data taken from NED. A '*' in the redshift column means that the redshift is taken as the average redshift of the cluster

In Fig. 6 the distribution of the likely and certain cluster dwarf elliptical galaxies located in the Fornax cluster is plotted as function of right ascension and declination, both in units of degrees.

The galaxies that have at least one detection in the W3 or W4 detection and a detection in at least one of the *Herschel* bands are represented by dots whose colour corresponds to the colour in the legend. NGC 1399 is also plotted and is represented by a yellow dot. The cone search radius of 4 degrees around NGC 1399 is also plotted.

In Fig. 7. the distribution of the dwarf elliptical galaxies in the Virgo cluster is shown. These galaxies are all certain or possible cluster members. The galaxies that have at least one detection in the W3 or W4 bands and a detection in at least one of the *Herschel* bands are represented by dots whose colour corresponds to the colour in the legend. The On the vertical axis the declination is plotted and on the horizontal axis the right ascension is plotted. Both are in units of degrees. The central elliptical galaxy M87 is also plotted and is represented by a yellow dot. The cone search radius of 6 degrees around M87 is also plotted.

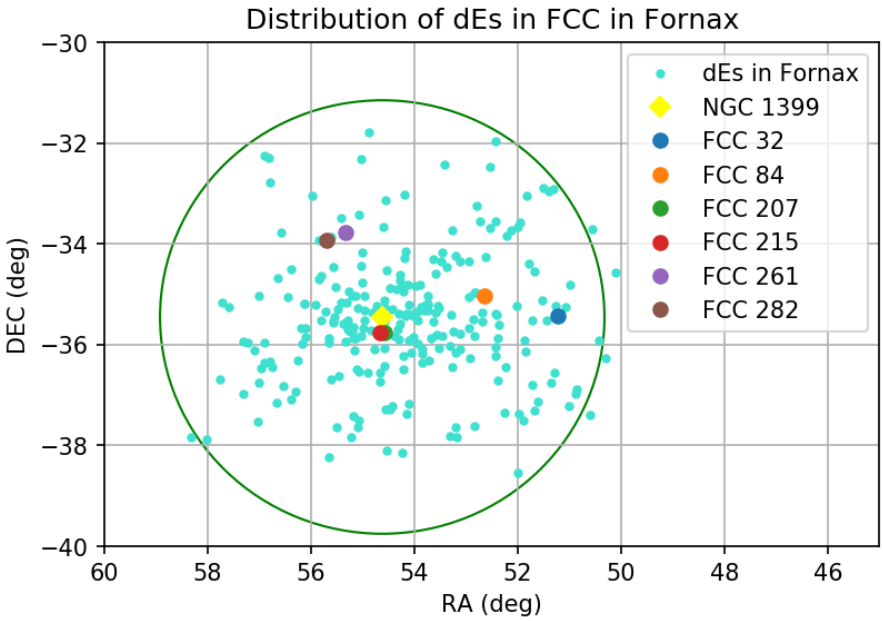

Figure 6: Plot of the distribution of the (likely) cluster members of the dwarf ellipticals in the Fornax cluster. The dwarf elliptical galaxies in the Fornax cluster with at least a W3 or W4 detection and at least one detection in the *Herschel* bands are represented by dots corresponding to the colours in the legend. The yellow dot in the plots represents the central galaxy NGC 1399. The smaller blue dots represents the likely or certain cluster dEs as presented in the FCC.

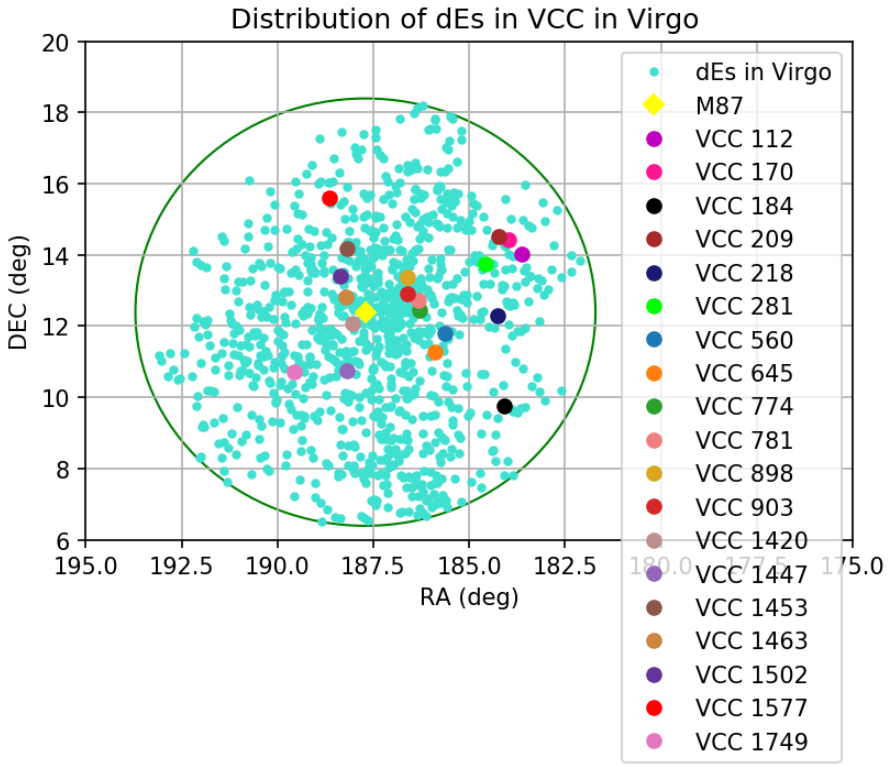

Figure 7: Plot of the distribution of the the (possible) dwarf ellipticals in the Virgo cluster . The dwarf galaxies in the Fornax cluster with at least a W3 or W4 detection and at least one detection in the *Herschel* bands are represented by dots corresponding to the colours in the legend. The yellow dot in the plots represents the central galaxy M87. The smaller blue dots represents the likely or certain cluster dEs as presented in the VCC.

3 SED modelling

SED modelling is used to determine some physical properties of the galaxy. A χ^2 minimising algorithm that minimises the difference between the measured set of fluxes and the modelled fluxes corresponding to the same wavelength is used. The SED fitting was done under the assumption that the emission comes from thermal dust only. The fitting was done using a Python environment. The python function 'curve-fit' was used to fit the function to the data points. The SED is a greybody at low frequencies and a power law at high frequencies. The form of a greybody function is also seen in the range between approximately 80 μm to 1000 μm in the SED in Fig. 5. This measures starburst emission in the whole galaxy (Casey, 2012). The power law for the mid-IR part corresponds to the hot dust emission from star burst regions (Casey, 2012). The equation for the IR SED is given in Eq. (1) (Wang et al., 2016):

$$S_\nu \propto \begin{cases} \nu^\beta B_\nu(T_d), & \text{if } \nu < \nu_0 \\ \nu^{-\gamma}, & \text{if } \nu \geq \nu_0 \end{cases} \tag{1}$$

where S_ν is the flux density, ν is the frequency, β is the emissivity constant and is fixed at 2. γ is the slope of the high frequency part of the SED and is taken to be 2 as in Wang et al. (2016). $B_\nu(T_d)$ is the blackbody function at the dust temperature T_d and is given by:

$$B_\nu(T_d) = \frac{2h\nu^3}{c^2} \frac{1}{\mathrm{e}^{\frac{h\nu}{kT_d}} - 1} \tag{2}$$

where h is the Planck constant, k is the Boltzmann constant, c is the speed of light. The constants are used in cgs units.

ν_0 as used in Eq. (1) is the frequency at which the greybody and the power law connect. This relation is needed to obtain a continuous transition between the power law and the greybody. ν_0 can be solved from Eq. (3) (Wang et al., 2016).

$$\frac{\mathrm{d}\ln[\nu^\beta B_\nu(T_d)]}{\mathrm{d}\ln\nu} = -\gamma \tag{3}$$

First the two parts of Eq. (1) need to become one function. The two functions both have their own normalisation constant, but they are related. Eq (1) is rewritten with the two normalisation constants, A and B:

$$S_\nu = \begin{cases} A \cdot \nu^\beta B_\nu(T_d), & \text{if } \nu < \nu_0 \\ B \cdot \nu^{-\gamma}, & \text{if } \nu \geq \nu_0 \end{cases} \tag{4}$$

The relation between A and B can be determined from the definition of a continuous function. The composite function needs to be continuous from the left as in Eq. (5) and from the right as in Eq. (6).

$$\lim_{\nu \to \nu_0^-} S_\nu(\nu) = S_\nu(\nu_0) \tag{5}$$

$$\lim_{\nu \to \nu_0^+} S_\nu(\nu) = S_\nu(\nu_0) \tag{6}$$

These two limits need to be equal. This results in an equation for B:

$$B = A \cdot \frac{\nu_0^\beta}{\nu_0^{-2}} \frac{2h\nu_0^3}{c^2} \frac{1}{\mathrm{e}^{\frac{h\nu_0}{kT}} - 1} \tag{7}$$

To do this SED fitting, an initial guess for the temperature and the normalisation constant, A, must be given. The normalisation constant also includes the conversion from erg $\mathrm{cm}^{-2}\mathrm{s}^{-1}\mathrm{Hz}^{-1}$ to mJy (which is a factor 10^{26}).

The wavelengths of the *WISE* and *Herschel* bands are converted to frequencies by:

$$\nu = \frac{c}{\lambda} \tag{8}$$

To correct for the redshift, z, Eq. (9) was used:

$$z = \frac{\lambda_{obs} - \lambda_{em}}{\lambda_{em}} \tag{9}$$

where λ_{obs} is the observed wavelength and λ_{em} is the emitted wavelength.

The flux in each *WISE* band was given in magnitudes and the magnitudes were converted to flux densities using Eq. (10) (Wright et al., 2010).

$$S_\nu = S_\nu^0 \cdot 10^{-M_\nu/2.5} \cdot 10^3 \tag{10}$$

where S_ν is the corresponding flux density in mJy and M_ν is the observed magnitude in the corresponding *WISE* band. S_ν^0 is the zero magnitude flux density for a given *WISE* band that corresponds to the response that Vega system gives. S_ν^0 depends on the assumed SED. Since the SED is assumed to be a power law with a power of -2 at high frequencies, S_ν^0 is equal to 306.682 Jy, 170.663 Jy, 29.045 Jy and 8.284 Jy for W1, W2, W3 and W4 respectively (Wright et al., 2010).

From the SED fitting the integrated infrared luminosity, L_{IR}, can be determined. The SED of the galaxy is integrated over the frequency range 8-1000 μm:

$$L_{IR} = 4\pi D_L^2 \int_{8\mu\mathrm{m}}^{1000\mu\mathrm{m}} S_\nu d\nu \tag{11}$$

where D_L is the luminosity distance to the cluster. Here it is assumed that the distance to the galaxy is approximately the same as the distance to the cluster. The distance to the clusters used are given in section 2.2.1 and 2.2.2 for the Fornax cluster and Virgo cluster respectively. From the integrated infrared luminosity, the star formation rate (SFR) can be deduced. A linear relation between the SFR and the L_{IR} is assumed (Mckean, 2017).

$$SFR(\mathrm{M}_\odot \mathrm{yr}^{-1}) = 1.71 \cdot 10^{-10} L_{IR}(\mathrm{L}_\odot) \tag{12}$$

where L_{IR} is given in units of solar luminosities and the SFR is given is solar masses per year.

Determining the SFR from infrared luminosity has advantages over determining the SFR from recombination lines and UV emission, since for these other SFR indicators, the dust attenuation must be taken into account (Hayward et al., 2014).

The dust mass, M_d, can be determined from another SED fitting. A greybody with a single temperature component is fitted to the *Herschel* data. For this SED fitting only galaxies that have two or more detections in the *Herschel* bands are taken into account. The equation that is fitted is:

$$S_\nu = \frac{\kappa_{abs}(\nu) M_d B_\nu(T_d)}{D^2} \tag{13}$$

Here T_d is the dust temperature obtained from the SED fitting of Eq. (1), D is the distance to the cluster and $\kappa_{abs}(\nu)$ is the dust absorption coefficient and is given by (Fuller et al., 2014):

$$\kappa_{abs}(\nu) = \kappa_{abs}(\nu_0) \left(\frac{\nu}{\nu_0}\right)^\beta \tag{14}$$

where $\kappa_{abs}(\nu_0)$ is the dust mass-opacity coefficient at 350 μm and is taken to be 1.92 $\mathrm{cm}^2\mathrm{g}^{-1}$ (Draine, 2003).

A rough estimate for the stellar mass, M_* is made using the relation which is the best fit relation found by Fuller et al. (2014).

$$\log\left(\frac{M_*}{M_\odot}\right) = -0.51 m_B + 16.6 \tag{15}$$

where m_B is the apparent blue magnitude of the galaxy.

4 Analysis and results of SED fitting

In this section the results of the SED modelling are described. Dust temperatures, infrared luminosities, star formation rates, dust masses and stellar masses will be deduces from this SED modelling. The results are presented here.

A sample of 6 galaxies in the Fornax cluster and 19 galaxies in the Virgo cluster have been detected. The SEDs of these galaxies were fitted using a composite function of a power law for low wavelengths and a single temperature greybody with emissivity β=2 for higher wavelengths.

The results of the SED fitting of the sample of 6 dwarf elliptical galaxies in the Fornax cluster are given in Fig. 8. The horizontal axis represents the rest frame wavelength in units of μm and

the vertical axis represents the flux density in units of mJy. The red error bars correspond to the data points. The results for the SED fitting for the 19 dwarf elliptical galaxies in the Virgo cluster are given in Fig. 9 in which the flux density in units of mJy is plotted versus the rest frame wavelength in units of μm.

From the SED fitting, T_d was estimated whereof L_{IR} and the corresponding SFR where deduced. In galaxies having two or more detections in the *Herschel* bands, M_d was determined using another SED fitting where T_d was determined in the SED fittings of Fig. 8 and Fig. 9 for the Fornax cluster and Virgo cluster respectively. The Fornax cluster sample has 4 dES having a detection in at least two *Herschel* bands. For these galaxies the SED fittings for determining the dust mass are shown in Fig. 10. The Virgo cluster sample also has 4 dEs which have a detection in at least two *Herschel* bands. The results for the SED fitting for determining the dust masses for these dEs is shown in Fig. 11. The stellar masses for the sample of 6 dEs in the Fornax cluster and 19 dEs in the Virgo cluster were also estimated from Eq. (15). These physical properties of sample of dwarf elliptical galaxies in the Fornax cluster and the Virgo cluster are given in Table 3 and Table 4 respectively. The uncertainties for dust temperatures and dust masses are originating from the χ^2 minimalisation algorithm. All other uncertainties are derived using propagation of uncertainties.

Object	T_d (K)	L_{IR} ($L_\odot$)	SFR ($M_\odot yr^{-1}$)	$\log(\frac{M_d}{M_\odot})$	$\log(\frac{M_*}{M_\odot})$
FCC 32	20.2 ± 2.9	7.8 ± 0.3	0.012 ± 0.006	5.4 ± 0.3	8.7
FCC 84	10.7 ± 1.0	7.4 ± 0.2	0.0041 ± 0.0010	6.5 ± 0.1	6.7
FCC 207	17.3 ± 2.0	7.3 ± 0.3	0.0033 ± 0.0015	-	8.5
FCC 215	11.6 ± 0.9	7.0 ± 0.2	0.0016 ± 0.0005	6.0 ± 0.1	6.8
FCC 261	16.9 ± 0.4	7.4 ± 0.2	0.0041 ± 0.0004	-	8.5
FCC 282	19.7 ± 1.0	8.1 ± 0.1	0.021 ± 0.004	5.7 ± 0.4	9.2

Table 3: Results for the sample of galaxies in the Fornax cluster. A '-' in one of the columns is displayed if the quantity could not be determined with the available data.

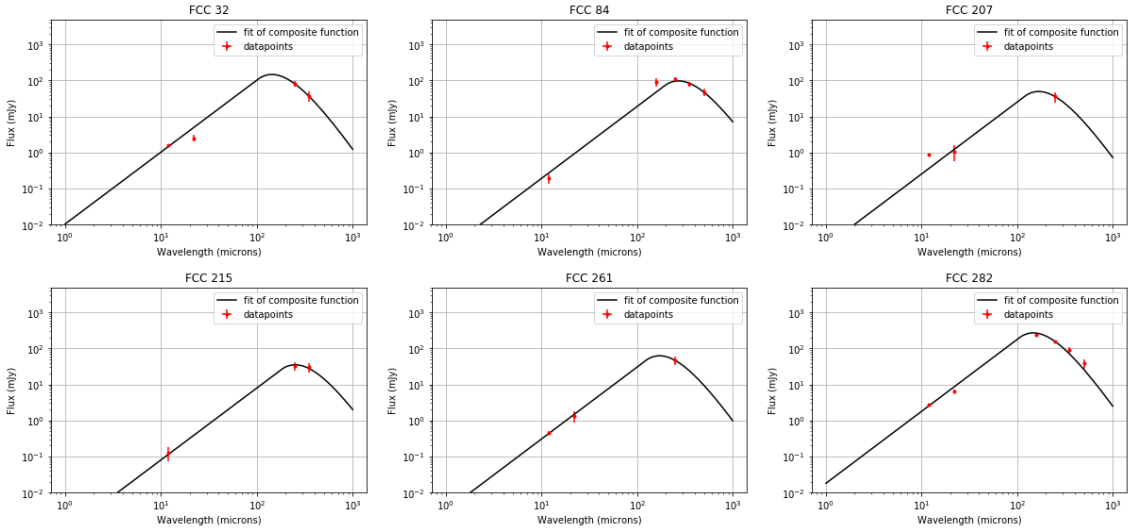

Figure 8: The Spectral Energy Distributions of the 6 Fornax dwarf elliptical galaxies with at least a W3 or W4 detection and at least one detection in the *Herschel* bands

Object	T_d (K)	L_{IR} ($L_\odot$)	SFR ($M_\odot yr^{-1}$)	$\log(\frac{M_d}{M_\odot})$	$\log(\frac{M_*}{M_\odot})$
VCC 112	13.2 ± 1.1	7.1 ± 0.3	0.0020 ± 0.0006	-	6.7
VCC 170	19.9 ± 0.6	7.7 ± 0.1	0.0079 ± 0.0009	5.3 ± 0.4	9.0
VCC 184	20.7 ± 1.2	7.7 ± 0.1	0.0076 ± 0.0017	-	8.3
VCC 209	17.7 ± 2.2	7.8 ± 0.3	0.011 ± 0.006	-	9.1
VCC 218	22.1 ± 1.0	7.5 ± 0.1	0.0053 ± 0.0010	-	9.0
VCC 281	18.0 ± 0.9	7.6 ± 0.2	0.0074 ± 0.0015	5.5 ±0.1	8.8
VCC 560	20.8 ± 1.1	7.2 ± 0.1	0.0026 ± 0.0006	-	7.9
VCC 645	20.4 ± 1.2	7.1 ± 0.3	0.0022 ± 0.0005	-	7.3
VCC 774	12.9 ± 1.9	7.3 ± 0.2	0.0033 ± 0.0010	-	7.2
VCC 781	19.7 ± 1.5	7.6 ± 0.2	0.0061 ± 0.0019	5.2 ± 0.1	9.2
VCC 898	20.1 ± 1.4	7.1 ± 0.3	0.0018 ± 0.0005	-	6.7
VCC 903	19.9 ± 1.0	7.1 ± 0.1	0.0021 ± 0.0004	-	7.0
VCC 1420	17.3 ± 3.1	7.4 ± 0.3	0.0038 ± 0.0027	5.3 ± 0.2	8.3
VCC 1447	21.1 ± 2.1	7.3 ± 0.1	0.0037 ± 0.0008	-	6.7
VCC 1453	20.7 ± 1.1	7.1 ± 0.1	0.0022 ± 0.0005	-	9.3
VCC 1463	17.8 ± 0.8	7.2 ± 0.2	0.0030 ± 0.0007	-	7.2
VCC 1502	13.9 ± 1.3	7.0 ± 0.2	0.0019 ± 0.0005	-	7.2
VCC 1577	15.9 ± 2.1	7.0 ± 0.2	0.0018 ± 0.0004	-	8.5
VCC 1749	20.1 ± 1.3	7.1 ± 0.1	0.0021 ± 0.0005	-	6.7

Table 4: Results for the sample of galaxies in the Virgo cluster. A '-' in one of the columns is displayed if the quantity could not be determined with the available data.

The mean dust temperature of the distribution of the sample of dwarf ellipticals in the Fornax cluster is 16.1 K ± 3.7 K, whereas the mean dust temperature for the sample of VCC dEs is 18.5 K ± 2.7 K. A comparison between dust temperatures in the clusters is shown in the histogram shown in Fig. 12. It seems that Fornax and Virgo have comparable dust temperatures although Fornax has outliers with lower dust temperatures and Virgo has outliers toward the higher dust temperatures.

A histogram for the star formation rate in the Fornax is shown in Fig. 13. Since the star formation rates are deduced from a linear relation between the integrated infrared luminosity and the star formation rate, the distribution of infrared luminosities would be the same as the distribution for star formation rates. Therefore the histograms would also be similar and a comparison between the galaxy clusters using one of these quantities is used. We chose to compare the star formation rates.

The mean SFR for the Fornax cluster is 0.0077 $M_\odot yr^{-1}$ ± 0.0068 $M_\odot yr^{-1}$ and the mean SFR for the Virgo cluster is 0.0041 $M_\odot yr^{-1}$ ± 0.0026 $M_\odot yr^{-1}$. From Fig. 13 can be seen that dEs with a $SFR < 0.008$ $M_\odot yr^{-1}$ are most common. Although the mean star formation rate is higher for the Fornax cluster dEs than for the Virgo cluster dEs, the star formation rates in Fornax and Virgo are comparable within the uncertainties. A discussion related to the higher star formation rate for the Fornax sample as compared to the Virgo sample is given below.

In comparison, the SFR of the Milky Way is 1.65± 0.19 $M_\odot yr^{-1}$ (Licquia and Newman, 2015). The Milky Way is a spiral galaxy which is believed to have a significant star formation rate. Moreover, a spiral galaxy is significantly larger than a dE. However, a dE does have a significant SFR.

The SFR of a starburst galaxy is on the order of a 100 $M_\odot yr^{-1}$ (Sparke & Gallagher, 2007). This number is significant higher than the star formation rates found for dEs. It can be concluded that a dE does not undergo a short period of an exceptionally high rate of star formation at this moment or in the recent past and is therefore not similar to a starburst galaxy.

Fig. 14 shows a histogram of the dust mass for the Virgo cluster and the Fornax cluster. In both galaxies 4 dwarf ellipticals are detected in at least 2 *Herschel* bands. The mean dust mass for these galaxies in the Fornax cluster is $< \log(\frac{M_d}{M_\odot}) >$=5.9 ± 0.5. For the Virgo cluster the mean dust mass for the 4 dwarf ellipticals was found to be $< \log(\frac{M_d}{M_\odot}) >$=5.3 ± 0.2. The dust masses for dwarf elliptical galaxies in both clusters are comparable within the uncertainties. A significant comparison cannot be made because of the low number of galaxies for which have at least two detections in the *Herschel* bands.

Fig. 15 shows the histogram for the rough estimates of the stellar masses of the galaxies. The stellar mass of the dEs is assumed to be dominated by the old stellar population since dEs are assumed to be gas- and dust poor galaxies. The mean stellar mass for the Fornax cluster is $< \log(\frac{M_*}{M_\odot}) >= 8.1 \pm 1.0$ and the mean stellar mass for the Virgo cluster is $< \log(\frac{M_*}{M_\odot}) >$=7.9 ± 1.0. The stellar masses of the sample of dwarf elliptical galaxies in the Fornax cluster and the Virgo cluster are comparable within the uncertainties.

The somewhat higher average star formation rate and integrated infrared luminosity for the sample located in the Fornax cluster as compared to the Virgo cluster can be explained by the types of galaxies present in the sample of FCC galaxies in the sample. FCC 32, FCC 261 and FCC 282 are classified as dE pec/BCD, dE3 pec / ImIv and ImIv/ dE pec respectively (see also Table 1), meaning that thee galaxies are not typical dEs. This corresponds to 50% ± 29% of the sample of dEs located in the Fornax cluster. However in the Virgo cluster sample only VCC 170 (dS0 pec) and VCC 281 (dS0/BCD) are not typical dEs, corresponding to 11% ± 7% of the VCC dEs in the sample.

A peculiar galaxy is characterised by unusual shapes, unusual amounts of gas and dust, higher or lower surface brightnesses compared to the galaxy types they are given and could even have features as nuclear jets (Sparke & Gallagher, 2007). If these peculiar and blue compact dwarf galaxies are taken out of the sample, the weighted average SFR of the sample in the Fornax cluster becomes 0.0022 $M_\odot yr^{-1}$ ± 0.0005 $M_\odot yr^{-1}$. The weighted average SFR for the Virgo cluster sample becomes 0.0024 $M_\odot yr^{-1}$ ± 0.0002 $M_\odot yr^{-1}$. The mean star formation rates deduced from the distribution are 0.0030 $M_\odot yr^{-1}$ ± 0.0011 $M_\odot yr^{-1}$ and 0.0024 $M_\odot yr^{-1}$ ± 0.0012 $M_\odot yr^{-1}$. Comparing these star formation rates, it can be concluded that star formation rates for normal dEs in the Fornax cluster and Virgo cluster are comparable within the uncertainties. For the other physical properties such a relation is not found although such a relation would be expected for the dust mass. However, if these peculiar galaxies are excluded only 2 galaxies in the Fornax cluster and 2 galaxies in the Virgo cluster remain and a meaningful comparison cannot be made.

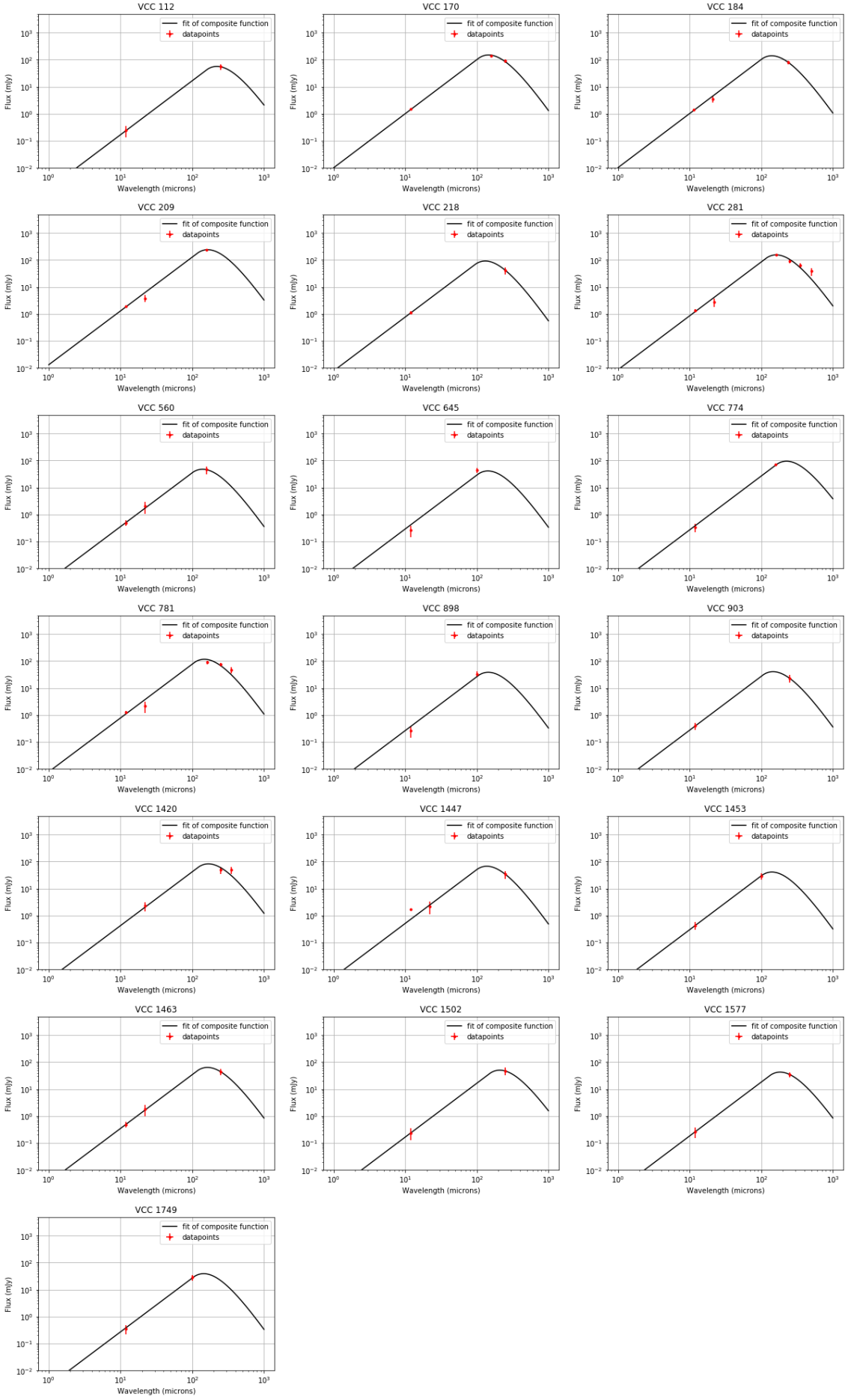

Figure 9: The Spectral Energy Distributions of the 19 Virgo dwarf elliptical galaxies with at least one detection in the W3 band or the W4 band and at least one detection in the *Herschel* bands

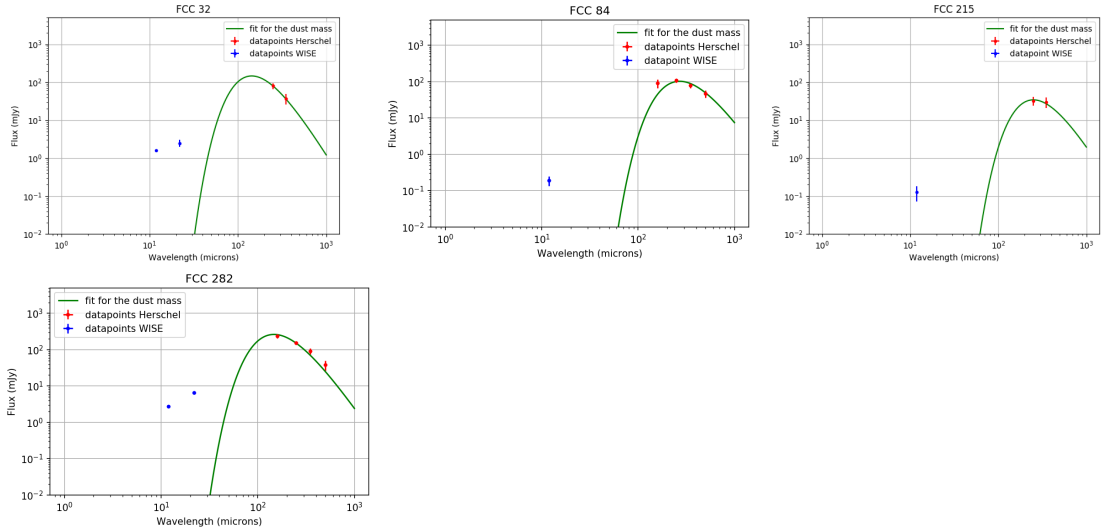

Figure 10: The Spectral Energy Distributions of the 4 Fornax dwarf elliptical galaxies in the sample that have at least two detections in the Herschel data. From this the dust mass is determined.The blue error bars correspond to the W3 and/or W4 data which are not fitted here. The the red error bars correspond to the available *Herschel* data. Only the *Herschel* data is taken into account for the fitting of the spectral energy distributions

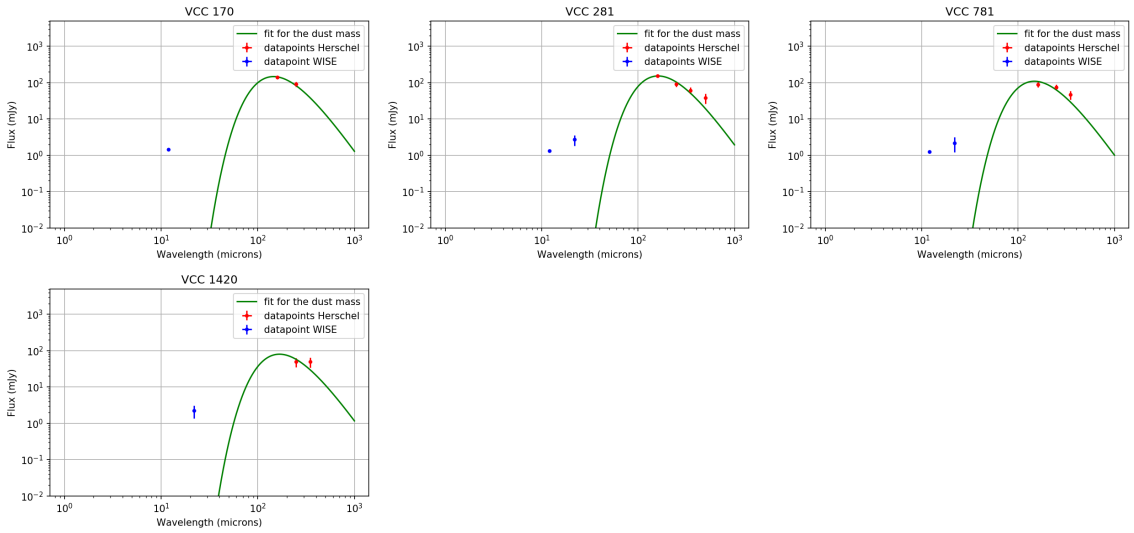

Figure 11: The Spectral Energy Distributions to determine the gas mass of the 4 Virgo dwarf elliptical galaxies in the sample that have at least two detections in the Herschel bands. The blue error bars correspond to the W3 and/or W4 data which are not fitted here. The red error bars correspond to the available *Herschel* data. Only the *Herschel* data is taken into account for the fitting of these spectral energy distributions

The SED fits for some galaxies are uncertain. For for FCC 32, FCC 84, FCC 207, VCC 209, VCC 645, VCC 781 and VCC 1447 the fits for the SEDs do not go through all data points. Part of these uncertainties in the fitting procedure is incorporated in the uncertainties for the physical quantities. The fit for the galaxies having only two detections is highly uncertain, since a fit with only two data points, one in either parts of the composite function, is uncertain. Moreover, VCC 1420 has a detection in the 250 μm band with a flux density that is equal to the flux density in the 350 μm band. Moreover, some SEDs do not have detections in all bands. The reason that not all galaxies are detected in all bands is in part due to the observation that dEs are hard to detect in the infrared since they have a low stellar mass and a low surface brightness. Therefore the dust-to-stellar mass ratio must be higher than for other morphology types in order to be able to detect the galaxy (Fuller et al., 2014).

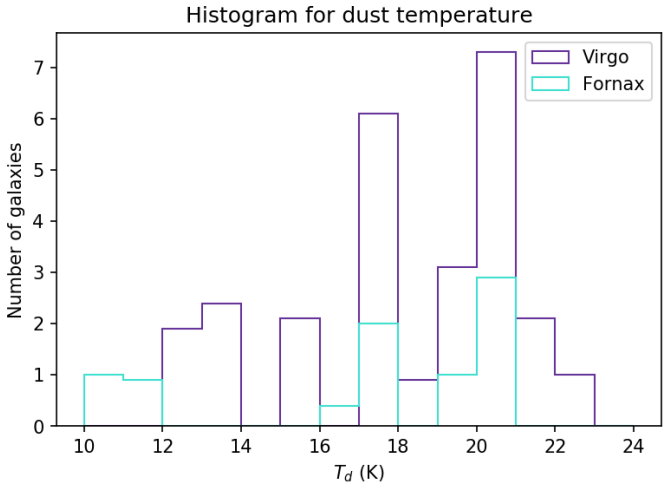

Figure 12: The histogram of the T_d of the Fornax cluster (turquoise) and the Virgo cluster (purple).

.

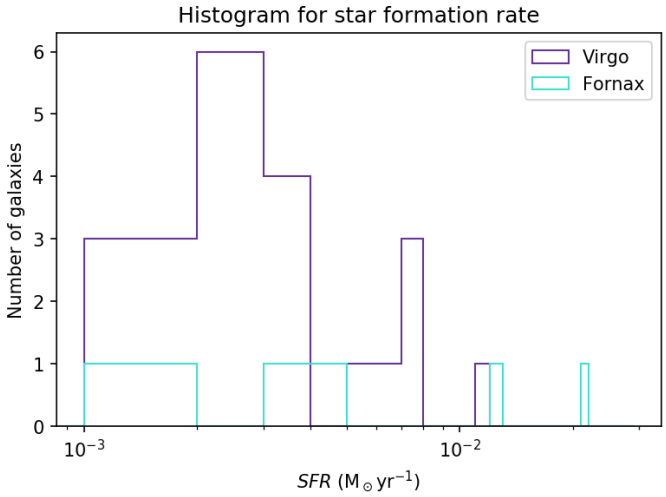

Figure 13: Histogram of SFR of the Fornax cluster (turquoise) and Virgo cluster (purple).

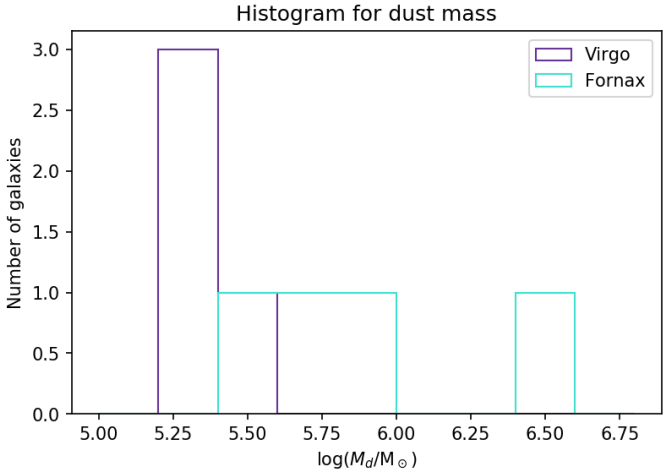

Figure 14: Histogram of M_d of the Fornax cluster (turquoise) and Virgo cluster (purple).

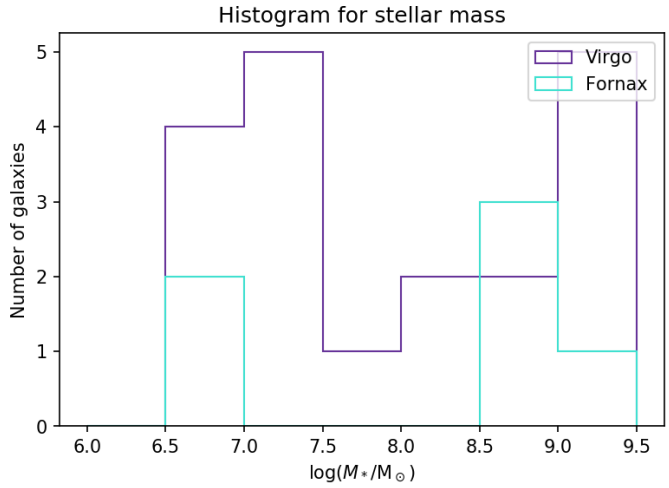

Figure 15: Histogram of M_* of the Fornax cluster (turquoise) and Virgo cluster (purple).

5 Discussion

In this section we describe some additional features and we look at the whether the location affects the fraction of galaxies with cold-warm ISM. We investigate whether the location where the galaxy is found in the cluster has an effect on the detection probability.

We accidentally had a spectrum available for FCC 207, from the the Sydney-Australian-Astronomical-Observatory Multi-object Integral-Field Spectrograph (SAMI) instrument on the The Anglo-Australian Telescope (AAT). It showed emission lines, something which is rather unusual for dEs. This emmision spectrum shows the presence of ionised gas, most likely ionised by recently formed stars. This spectrum can be seen in Fig. 16.

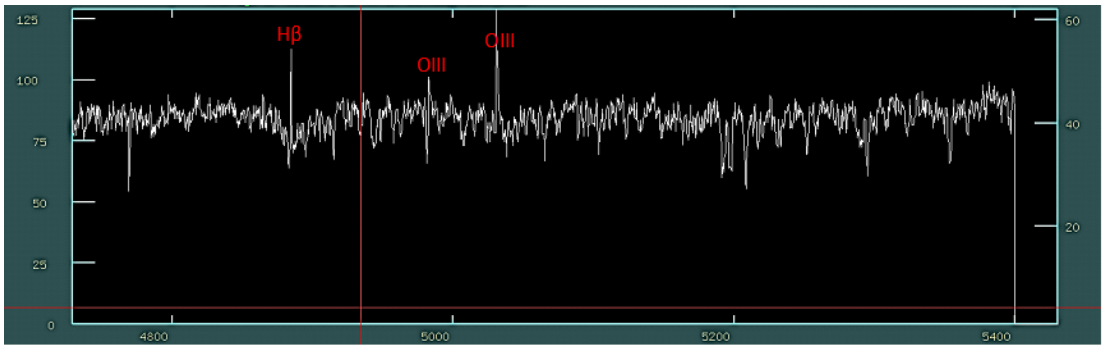

Figure 16: Emission spectrum of FCC 207. The spectral lines belonging to the different emission lines are also shown

5.1 Location of the galaxy in the cluster

Is there a relation between the detection probabilities and the location where the galaxy is found in the cluster? We detected 6 dEs in the Fornax cluster having a W3 and/or W4 detection and a detection in one of the *Herschel* bands. This corresponds to 3% ± 1% of the dEs catalogued in the FCC as certain or likely cluster members and located within a radius of 4° from NGC 1399. 19 dEs in the Virgo cluster having a W3 and/or W4 detection and a detection in one of the *Herschel* bands are detected. This is 2% ± 1% of dES catalogued in the VCC as certain or possible cluster members which are located within a radius of 6 ° of M87.

Half the search radius around the central galaxies of the clusters is used to distinguish two regions. The galaxies that are located within a radius of 2° of NGC 1399 are considered to be located close to the center of the Fornax cluster. The galaxies outside this radius are considered to be located in the outskirts of the Fornax cluster. Similarly, galaxies that are located within a radius of 3° of M87 are considered to be located in the denser parts of the Virgo cluster, whereas the galaxies located outside this radius are considered to be located toward the outskirts of the cluster.

The radii from the center of the galaxies in the sample of 6 FCC galaxies and 19 VCC galaxies are shown in the last columns of Table 1 and Table 2 for the Fornax cluster and the Virgo cluster respectively.

For the dEs considered to be possible or certain cluster members of the Fornax cluster, 150 galaxies are located in the inner 2° the cluster core, corresponding to 60% ± 5% (see also Fig. 6). The other 101 galaxies are located in the outer parts of the cluster, corresponding to 40% ± 4% of the dEs considered to be possible or certain cluster members of the Fornax cluster. We detect 4 out of the 6 detected dEs in the inner 2° of the Fornax cluster, corresponding to 3% ± 2% of the number of dEs in the sample located in the inner region of the Fornax cluster. 2 dEs are detected that are located in the regions between 2° and 4° from NGC1399. This corresponds to 2% ± 1% of the sample of dEs located in the outer region.

537 VCC dwarf ellipticals are located in the inner 3°, corresponding to 51% ± 3% of the dwarf ellipticals in the Virgo cluster (see also Fig. 7). 12 out of the 19 dEs that we detected are located in the inner region of the Virgo cluster. This corresponds to 63% ± 11% of the detected galaxies in the Virgo cluster and 2% ± 1% of the galaxies located in the inner region of the Virgo cluster. 512 VCC dEs are located in the region between 3° and 6° from M87, corresponding to 49% ± 2% of the dEs that are certain or possible members of the Virgo cluster. We detected 7 of these galaxies, corresponding to 1.4% ± 0.6% of the dEs located in the outer parts.

In the inner parts of the clusters of galaxies there are relatively more detections in the W3 and/or W4 and in at least one of the *Herschel* bands compared to the outer regions of the clusters. This is probably due to the environmental effects that take place more in the inner regions of the cluster.

5.2 Comparisons with other work

5.2.1 Lisker et al.: Blue centers

Lisker et al. (2006b) discovered some dEs in the Virgo cluster with blue centers which they classified as dE(bc). These blue centers indicate recent or ongoing star formation. They used the optical imaging data of the Sloan Digital Sky Survey (SSDS) Data Release 4, which covers almost all galaxies catalogued in the VCC except for a small area which is also not covered in our search radius of 6 degrees around M87. They took into account the certain or possible cluster members catalogued in the VCC which have $m_B < 18$. This corresponds to the limit to which the VCC is considered to be complete. Their sample consists of 552 dEs catalogued as certain or possible cluster members. Here they took into account revised membership and classifications from Binggeli et al. (1993) and revised classifications of Geha et al. (2003) and Lotz et al. (2004). We did not take into account these revised classifications. They excluded galaxies that are possible irregular galaxies and 25 dEs that are not covered by the SSDS. This resulted in a sample of 476 dEs. They found 23 out of 476 (5% ± 1%) dEs with significant positive colour gradients.

Galaxies detected in this work and classified by Lisker et al. as dE(bc) are VCC 170, VCC 218, VCC 281 and VCC 781. These galaxies are classified as dS0's by Binggelli et al. (1985). 21% ±

10% of the sample of 19 galaxies are classified as dE(bc). In this work we detected 17% ± 9% of the galaxies classified as dE(bc) by Lisker et al.

In their first paper in the series Lisker et al. (2006a) found early-type elliptical galaxies with disks or other substructures. Other substructures mean boxy features or irregular or clumpy central features which are likely caused by gas and dust (Lisker et al., 2006a). Galaxies detected in this work and classified by Lisker et al. to have substructures other than disks are VCC 170, VCC 209, VCC 281 and VCC 781. These galaxies show higher than average SFR in our research.

It can be concluded that the sample that we considered and the sample that Lisker et al. considered are very different. Therefore not all dE(bc) are detected in our work and some galaxies are not in their sample, because restricted themselves to limit to which the VCC was considered to be complete (i.e. $m_B < 18$). The significant higher star formation rates for VCC 170, VCC 209, VCC 218, VCC 281 and VCC 781 are explained to the blue central features and the presence of substructures.

5.2.2 di Serego Alighieri et al.: dEs in Virgo

di Serego Alighieri et al. (2013) examined the dust content of early-type galaxies in the Virgo cluster, including some early-type dwarf elliptical galaxies. They searched for FIR radiation in a sample of 910 galaxies using 250 μm images of the *Herschel* Virgo Cluster Survey which covers an area of approximately 55 square degrees covered by 4 tiles and thus different from our sample. This survey is a confusion limited imaging survey (di Serego Alighieri et al., 2013). Both our study and the study by di Serego Alighieri et al. did not limit their search to $m_B < 18$. Their analysed sample consist of 52 early-type galaxies that have a reliable FIR detection. In their sample 20 galaxies are dEs. They reported a dust detection rate for the early-type dwarf elliptical galaxies of 3%. Here they took only the optically complete input sample and took into account a completeness limit of 24.3 mJy at 250 μm. We found 19 dEs located in the Virgo cluster that are detected in the 250 μm band. This corresponds to 2% ± 1% of the dEs in our main sample. These detection rates are in line to each other, although we do take into account these limits.

Using SED modelling they determined dust temperatures and dust masses. Their SED is a single temperature greybody, similar to what we used to fit the *Herschel* data. They also estimated stellar masses using broadband photometry in the optical range and in the near infrared, which is different from our assumed linear relationship between the stellar mass and the apparent blue magnitude (see Eq. (15)). In their sample 3 of the dEs detected in our sample are examined: VCC 209, VCC 218 and VCC 1420. For VCC 209 they report a dust temperature of 17.9 ± 0.6 K, a dust mass of $\log(\frac{M_d}{\mathrm{M}_\odot}) = 5.9 \pm 0.1$ and a stellar mass of $\log(\frac{M_*}{\mathrm{M}_\odot}) = 8.5 \pm 0.2$. For VCC 218 they report a dust temperature of 17.6 K (without uncertainty because a fixed value for the dust temperature for the SED fitting is used), a dust mass of $\log(\frac{M_d}{\mathrm{M}_\odot}) = 5.3 \pm 0.1$ and a stellar mass of $\log(\frac{M_*}{\mathrm{M}_\odot}) = 8.4 \pm 0.3$. For VCC 1420 they report a dust temperature of 16.3 ± 1.2 K, a dust mass of $\log(\frac{M_d}{\mathrm{M}_\odot}) = 5.7 \pm 0.2$ and a stellar mass of $\log(\frac{M_*}{\mathrm{M}_\odot}) = 8.1 \pm 0.2$. These results correspond to our research within 1σ.

From their initial sample they excluded dwarf elliptical galaxies that do not have available radial velocity data (and thus redshift data). We detected, however, a lot of dEs in the Virgo cluster that do not have available redshift data (see also Table 2).

5.2.3 Fuller et al.: dEs in Fornax

Fuller et al. (2014) determined FIR properties of galaxies in the Fornax cluster using the *Herschel* Fornax Cluster Survey, which covers a tile of 4°× 4° tile centered on NGC 1399. Their covered

area is a little bit bigger than our covered area, since we use a cone search radius of 4°. Using SED modelling, they determined dust temperature, dust mass and detection rates. They considered a sample of 237 FCC galaxies that fall into the SPIRE maps and divided these galaxies in different morphologies. They derived the flux densities by using the images of the galaxies. They detected 13 dwarf elliptical galaxies in the Fornax cluster in the 250 μm band. This corresponds to a detections rate of 6% ± 2% of the dEs in the Fornax cluster. Of our SPIRE data 7 dwarf elliptical galaxies in the Fornax cluster have a detection in the 250 μm band. This corresponds to a detection rate of 2.8 % ± 0.5 %. These values are significant lower than those reported by Fuller et al., which is in part due to the larger number of FCC galaxies taken into account. Another difference is that Fuller et al. determined the flux densities from the SPIRE images and took into account upper limits, where we considered a catalogue containing these flux densities and did not consider upper limits to the flux densities.

Fuller et al. determined dust temperatures, dust masses for galaxies having at least 3 *Herschel* detections using SED modelling. Although the function for their greybody was different from our composite function, the greybody parts of the SED are similar. Both our study and the study done by Fuller et al. determined dust temperatures and dust masses for FCC 215, FCC 261 and FCC 282. However, Fuller et al. classified FCC 261 and FCC 282 as irregular galaxies. From their paper it is not clear where the morphological classification originates from. Fuller et al. found a dust temperature of 15.78 K ± 1.35 K and a dust mass of $\log\left(\frac{M_d}{M_\odot}\right)$= 6.13 ± 0.15 for FCC 261. In this research the dust temperature found corresponds within the uncertainties to what was found by Fuller et al. We could not determine the dust mass for FCC 261 because the PACS and SPIRE point source catalogues do not provide detections for FCC 261. For FCC 282 a dust temperature of 18.04 ± 0.8 K and a dust mass of $\log(\frac{M_d}{M_\odot})$ =5.83 ± 0.09 was found by Fuller et al. These results agree with our results within the uncertainties. For FCC 215 Fuller et al. found a dust temperature of 15.64 K ± 0.08 K and a dust mass of $\log(\frac{M_d}{M_\odot})$= 5.23 ± 0.84. The dust temperature for FCC 215 determine by Fuller et al. is significant higher than the dust temperature we determined. The dust temperature for FCC 215 found by Fuller et al. has a very small uncertainty. Their fit for FCC 215, however, has a high χ^2 value which makes the fit uncertain.

We used the same technique to determine the stellar masses as Fuller et al. and the stellar masses determine by Fuller et al. for these three galaxies correspond to our results. However, where we used the apparent blue magnitudes catalogued in the FCC, they used those catalogued in *Hyperleda*.

They detected 2 more dEs in at least 3 *Herschel* bands: FCC 313 and FCC 48. We excluded FCC 48 because there was no *Herschel* data available for FCC 48 in the PACS and SPIRE point source catalogues, probably because of confusion. FCC 313 was excluded because of the lack of detections in the W3 and W4 bands. They also detected galaxies in more bands since they took into account the upper limits for the flux densities which they calculated from the 3σ noise in the point spread function convolved map. We have detected 3 more dwarf elliptical galaxies for which dust temperatures, dust masses, star formation rates and stellar masses where determined. By inspecting the online data Fuller et al. released, is was found that they also detected FCC 32 and FCC 207. However they only detected these in 2 *Herschel* bands, while their criteria for SED modelling is having at least 3 detections in the *Herschel* bands. For FCC 84 only upper limits are found by Fuller et al. Another difference between their work and our work is that they used the Herschel Fornax Cluster Survey for which FIR maps are reduced and we used the PACS and SPIRE point source catalogues archived in IRSA.

5.2.4 Buyle et al.: HI detections

In addition, Buyle et al. (2005) reported that the dwarf elliptical galaxies FCC 32 and FCC 336 have HI detections. They reported a total HI mass of 5.0 $\pm 1.7 \times 10^7 h_{75}^{-2} \mathrm{M}_\odot$ for FCC 32. The HI detection means that FCC 32 has a significant ISM. This means that the high star formation rate reported for FCC 32 can be explained by the detection of HI. Although considered in the FCC as a certain cluster member of the Fornax cluster, FCC 336 was not considered in our study since it has no W3, W4 or *Herschel* detections as catalogued in the used databases archived in IRSA.

6 Conclusion

Using data taken with the Wide-Field Infrared Survey Explorer and *Herschel* Space Observatory physical properties of 6 dwarf elliptical galaxies (dEs) in the Fornax cluster and 19 dwarf elliptical galaxies in the Virgo cluster were determined. The data was archived in the NASA/IPAC Infrared Science Archive and includes the All-Sky data Release of the *WISE* spectrograph and the point source catalogues of the Photoconductor Array Camera and Spectrometer (PACS) and the Spectral and Photometric Imaging Receiver (SPIRE) of *Herschel*. These catalogues are used in order to determine the flux densities needed in the spectral energy distribution (SED) modelling. 6 galaxies in the Fornax cluster and 19 galaxies in the Virgo cluster have a detection in the 12 μm band and/or the 22 μm band of the *WISE* spectrograph and at least one detection in the *Herschel* bands.

For these 6 dwarf elliptical galaxies in the Fornax cluster, the mean dust temperature $< T_d >=$ 16.1 K $\pm$ 3.7 K. For the 19 dwarf elliptical galaxies in the Virgo cluster, $< T_d >=$ 18.5 K $\pm$ 2.7 K. The mean star formation rate is 0.0077 $\mathrm{M}_\odot \mathrm{yr}^{-1}$ $\pm$ 0.0068 $\mathrm{M}_\odot \mathrm{yr}^{-1}$ for the detected Fornax cluster dEs and the mean SFR for the detected Virgo cluster dES is 0.0041 $\mathrm{M}_\odot \mathrm{yr}^{-1}$ $\pm$ 0.0026 $\mathrm{M}_\odot \mathrm{yr}^{-1}$. Although these star formation rates are comparable within the uncertainties, the somewhat higher star formation rate for the sample of dEs in the Fornax cluster can be explained by the relatively high contribution of peculiar dwarf elliptical in the Fornax cluster sample as compared to the Virgo cluster. If the possible blue compact dwarfs and peculiar dwarf ellipticals are excluded, the average star formation rates for the dEs located in Fornax are even more similar to the average star formation rates for dEs located in Virgo.

The mean dust masses for the 4 Fornax cluster dEs and 4 Virgo cluster dEs having at least two detections in the *Herschel* bands are $< \log(\frac{M_d}{\mathrm{M}_\odot}) >= 5.9 \pm 0.5$ and $< \log(\frac{M_d}{\mathrm{M}_\odot}) >= 5.3 \pm 0.2$ respectively. The mean stellar masses for the dEs in the Fornax cluster and the Virgo cluster are $< \log(\frac{M_*}{\mathrm{M}_\odot}) >= 8.1 \pm 1.0$ and $< \log(\frac{M_*}{\mathrm{M}_\odot}) >= 7.9 \pm 1.0$ respectively. These stellar masses are comparable within the uncertainties.

It can be concluded that the physical properties of dust in Fornax cluster dEs and Virgo cluster dEs are similar and therefore the environmental differences between Fornax and Virgo do not contribute to the physical properties of dust in these clusters. Moreover, there is significant amount of ISM present in these dwarf ellipticals, which is not expected because of the environmental processes that should take place.

A relation between the detection probabilities and the location where the galaxy is found in the cluster was established. The probability that a dwarf elliptical galaxies detected in our study is located in the inner half region of our search radii of 4° and 6° of the central galaxies of the Fornax cluster and Virgo cluster respectively, is higher than the probability that these dEs are found outside these half radii.

Comparisons with other work show that the physical properties we found are similar to the physical properties that are found. However the light infrared luminosities and star formation rates

have not been deduced in similar studies. However, some dEs with show significant ISM tracers are not found before in similar studies, mostly because others excluded galaxies with $m_B > 18$ or used different search radii.

For further research the upper limits for the *Herschel* Space Observatory could be taken into account. From there the dust masses, the gas masses of some of these galaxies could be estimated as well. Moreover, it would also be better to take into account revised catalogues for morphological classifications and membership of the galaxies (e.g. the revised memberships and morphologies determined by Binggeli (1993) and revised morphological classifications of Geha et al. (2003) and Lotz et al. (2004) for the Virgo cluster).

References

Arp H. (1988) *What is the mean redshift of the Virgo cluster?*, Astronomy and Astrophysics, 202: 70-75

Binggeli B., A. Sandage, G. A. Tammann (1985), *STUDIES OF THE VIRGO CLUSTER. II. A CATALOG OF 2096 GALAXIES IN THE VIRGO CLUSTER AREA*, The Astronomical Journal, 90: 9

Blakeslee J.P., A. Jordan, S. Met et al. (2009) *The ACS Fornax Cluster Survey. V. Measurement and Recalibration of Surface Brightness Fluctuations And A Precise Value Of The Fornax-Virgo Relative Distance*, Astrophysical Journal 694: 556-572

Boselli A., S. Boissier, L. Cortese, G. Gavazzi (2008), *The origin of the* $< \mu_e > -MB$ *and Kormendy relations in dwarf elliptical galaxies*, Astronomy and Astrophysics, 489: 1015-1022

Boselli A., J. C. Cuillandre, M. Fossati et al. (2016), *Spectacular tails of ionized gas in the Virgo cluster galaxy NGC 4569*, Astronomy and Astrophysics, 587:7

Buyle P., S. De Rijcke, D. Michielsen, M. Baes, H. Dejonghe (2005), *The HI content of Fornax dwarf elliptical galaxies: FCC032 and FCC336*, Monthly Notices of the Royal Astronomical Society, 360:853-858

Casey, C.M (2012), *Far-infrared Spectral Energy Distribution Fitting for Galaxies Near and Far*, Monthly Notices of the Royal Astronomical Society, 425:3094-3103

di Serego Alighieri, S., S. Bianchi, C. Pappalardo (2013), *The Herschel Virgo Cluster Survey. XIII. Dust in early-type galaxies*, Astronomy and Astrophysics, 552:A8

Draine B.T. (2003), *Interstellar Dust Grains*, Annu. Rev. Astron. Astrophys, 41:241–89

Dressler A. (1980), *Galaxy morphology in rich clusters - Implications for the formation and evolution of galaxies*, Astrophysical Journal, 236, pp. 351-365

Drinkwater M. J., S. Phillipps, J. B. Jones et al. (2000) *The Fornax Spectroscopic Survey*, Astronomy and Astrophysics, 355:900

Drinkwater M. J., M. D. Gregg, M. Colless (2001), *Substructure and Dynamics of The Fornax Cluster*, The Astrophysical Journal, 548:L139–L142

Drinkwater M. J. M. D. Gregg, B. A. Holman, M. J. I. Brown (2001b), *The evolution and star formation of dwarf galaxies in the Fornax cluster*, Monthly Notions of Royal Astronomy Society, 326: 1076-1094

Fuller C., J.I. Davies, R. Auld et al. (2014), *The Herschel Fornax Cluster Survey II: FIR properties of optically-selected Fornax cluster galaxies*, Monthly Notices of the Royal Astronomical Society, 440: 1571-1589

Ferguson H. C. (1989), *Population Studies in Groups and Clusters of Galaxies. II. A Catalog of Galaxies in the central* 3.5° *of the Fornax Cluster*, Astronomical Journal, 98: 2

Gunn, J. E., R. J. Gott (1972), *On the Infall of Matter Into Clusters of Galaxies and Some Effects on Their Evolution*, Astrophysical Journal, 176: 1

Grossi. M., L.K. Hunt, S.C. Madden et al. (2015), *The Herschel Virgo Cluster Survey. XVIII. Star-forming dwarf galaxies in a cluster environment*, Astronomy and Astrophysics, 574: A126

Hayward C. C., L. Lanz, M. L. N. Ashby et al. (2014) *The total infrared luminosity may significantly overestimate the star formation rate of recently quenched galaxies*, Monthly Notices of the Royal Astronomical Society, 445:1598 -1604

IRSA (2017), *About IRSA*, http://irsa.ipac.caltech.edu/about.html, consulted on June 12 2017

Lisker T., E. K. Grebel, B. Binggeli (2006a), *Virgo Cluster Early-Type Dwarf Galaxies With The Sloan Digital Sky Survey. I. On The Possible Disk Nature Of Bright Early-Type Dwarfs*, The Astronomical Journal, 132: 497–513

Lisker T., K. Glatt, P. Westera, E. K. Grebel (2006b), *Virgo Cluster Early-Type Dwarf Galaxies With The Sloan Digital Sky Survey. II. Early-Type Dwarf With Central Star Formation*, The Astronomical Journal, 132:2432-2452

Lisker T., E. K. Grebel, B. Binggeli, K. Glatt (2007), *Virgo Cluster Early-Type Dwarf Galaxies With The Sloan Digital Sky Survey. III. Subpopulations: Distributions, Shapes, Origins*, The Astrophysical Journal 660: 1186-1197

Licquia T. C., J. A. Newman (2015), *Improved Estimates of the Milky Way's Stellar Mass and Star Formation Rate from Hierarchical Bayesian Meta-Analysis* The Astrophysical Journal, 806: 1

Mamon, G. A., T. Sanchis, E. Salvador-Solé, J. M. Solanes (2004), *The origin of HI-deficiency in galaxies on the outskirts of the Virgo cluster. I. How far can galaxies bounce out of clusters*, Astronomy and Astrophysics, 414: 445-451.

Marton G., L. Calzoletti, a. M. Perez Garcia et al. (2017), *The Herschel*/PACS Point Source Catalogue Explanatory Supplement*

Mayer, L., F. Governato, M. Colp et al. (2001), *The Metamorphosis of Tidally Stirred Dwarf Galaxies*, The Astrophysical Journal, 559: 754-784

Mei, S., J. Blakeslee, P. Cote et al. (2007), *The ACS Virgo Cluster Survey. XIII. SBF Distance Catalog and the Three-Dimensional Structure of the Virgo Cluster*, Astrophysical Journal, 655:144-162

Meixner, M., F. Galliano, S. Hony et al. (2010),*HERschel Inventory of The Agents of Galaxy Evolution (HERITAGE): The Large Magellanic Cloud dust**, Astronomy and Astrophysics, 518: L71

Moore, B., N. Katz, G. Lake, A. Dressler, A. Oemler (1996), *Galaxy harassment and the evolution of clusters of galaxies*, Nature, 379: 613-616

Mckean, J. (2017), *Continuum emission mechanisms*, Introduction to Radio Astronomy

Sandage, A., B. Binggeli (1984), *Studies of the Virgo Cluster III. A Classification System and An Illustrated Atlas of Virgo Cluster Dwarf Galaxies*, The Astronomical Journal, 89: 7

Schultz, B., G. Marton, I. Valtchanov et al. (2007) *SPIRE Point Source Catalog Explanatory Supplement*

Skillman, E., E. Tolstoy, A. A. Cole et al. (2003), *Deep Hubble Space Telescope Imaging of IC 1613. II. Star formation History*, The Astropysical Journal, 596:253-272

Sparke L. S., J.S. Gallagher (2007): *Galaxies in the Universe: An Introduction*: second edition; Cambridge University Press, Cornwall

Wang L., P. Norberg, M.L.P. Gunawardhana et al., (2016) *GAMA/H-ATLAS: Common star-formation rate indicators and their dependence on galaxy physical parameters*, Monthly Notice Royal Astronomy

Wright E. L., P. R. M. Eisenhardt, A.K. Mainzer et al. (2010), *The Wide-Field Infrared Survey Explorer (WISE): Mission Description and Initial On-Orbit Performance*, The Astronomical Journal, 140: 1868-1881

A Appendix 1

All galaxies in the Virgo cluster having at least one detection in the W3 and W4 band and at least one *Herschel* detection are selected. The following FCC numbers have detections in at least one of the *Herschel* bands, but no W3 or W4 detection: 155, 251, 269, 313, 330. The following galaxies in the Fornax cluster are not used for the SED fitting because no available *Herschel* data in the PACS and SPIRE point source catalogues: 11, 17, 34, 42, 43, 46, 48, 51, 54, 57, 66, 69, 74, 76, 78, 80, 92, 99, 100, 101, 105, 106, 116, 124, 129, 136, 150, 154, 162, 163, 168, 174, 180, 195, 198, 202, 203, 204, 206, 217, 242, 243, 250, 253, 265, 266, 278, 279 and 294.

All galaxies in the Virgo cluster having at least one detection in the W3 and W4 band and at least one *Herschel* detection are selected. From this sample some galaxies do not have detections in the W3 or W4 bands. The following galaxies are therefore excluded: VCC 173, 216, 361, 490, 493, 608, 634, 646, 745, 750, 751, 779, 916, 990, 1010, 1033, 1163, 1225, 1227, 1407, 1441, 1444, 1501, 1528, 1549, 1669, 1684, 1755, 1912 and 1991

The following galaxies do not have available *Herschel* data in the PACS and SPIRE point source catalogues but have available W3 and/or W4 detections and are not used. The list of VCC numbers that are not used for this reason are given below. 37, 68, 82, 88, 90, 108, 139, 149, 184, 216, 227, 245, 285, 301, 305, 353, 354, 361, 372, 398, 414, 431, 437, 463, 466, 493, 498, 504, 540, 543, 560, 563, 569, 592, 608, 622, 634, 634, 643, 645, 646, 652, 659, 673, 678, 694, 705, 716, 723, 726, 745, 748, 750, 755, 765, 775, 777, 779, 786, 797, 815, 823, 832, 833, 856, 860, 882, 893, 896, 920, 922, 924, 932, 965, 976, 982, 990, 991, 994, 999, 1000, 1023, 1031, 1033, 1036, 1039, 1057, 1059, 1073, 1075, 1075, 1078, 1081, 1087, 1111, 1129, 1162, 1163, 1198, 1215, 1224, 1225, 1227, 1235, 1239, 1252, 1292, 1296, 1298, 1319, 1323, 1328, 1334, 1340, 1395, 1396, 1407, 1417, 1433, 1441, 1444, 1467, 1491, 1493, 1506 1520, 1531, 1549, 1590, 1594, 1606, 1626, 1639, 1649, 1659, 1667, 1669, 1674, 1682, 1694, 1702, 1708, 1714, 1740, 1747, 1755, 1795, 1815, 1828, 1852, 1867, 1874, 1877, 1890, 1905, 1910, 1919, 1924, 1941, 1942, 1966, 1990, 1991, 2022, 2028, 2035, 2061, 2081, 2090.